Electronic supplementary information

Stabilizing $LiCoO_2$ at 4.6 V by regulating the anti-oxidative solvents

Hengyu Ren[a,‡], Guorui Zheng[a,b,‡,], Yuhang Li[b], Shiming Chen[a], Xiaohu Wang[a], Mingzheng Zhang[a], Wenguang Zhao[a], Haocong Yi[a], Weiyuan Huang[c], Jianjun Fang[a,d], Tongchao Liu[c], Luyi Yang[a], Ming Liu[b,*], Qinghe Zhao[a,*], and Feng Pan[a,*]*

[a]School of Advanced Materials, Peking University Shenzhen Graduate School, Peking University, Shenzhen 518055, P. R. China.

[b]Institute of Materials Research, Tsinghua Shenzhen International Graduate School, Tsinghua University, Shenzhen 518055, P. R. China.

[c]Chemical Sciences and Engineering Division, Argonne National Laboratory, Lemont, IL 60439, USA.

[d]Qiantu battery Technology Co., Ltd, Dongguan 523808, P. R. China.

[‡]These authors contributed equally.

[*]Corresponding authors. E-mail: zhengguorui1991@163.com (G. Z.); liuming@sz.tsinghua.edu.cn (M. L.); zhaoqh@pku.edu.cn (Q. Z.); panfeng@pkusz.edu.cn (F. P.).

Table of Contents

Experimental section.....Pages 3-5

Figs. S1-S42.....Pages 6-47

Tables S1-S4.....Pages 48-52

References.....Pages 53

Experimental section

Electrodes and electrolytes preparation

The commercial LCO cathode is a typical high-voltage LCO, with doping elements of 4000 ppm Al, and 1500 ppm Mg, etc., and with a D50 value of 4.5 μm. The cathode electrodes used in the coin-type (CR2032) half cells were prepared by mixing LCO active material, acetylene black (AB) and polyvinylidene difluoride (PVDF) binder at a weight ratio of 8:1:1. The slurry was then cast onto an Al foil and dried at 100 °C overnight to obtain the electrodes. Then electrodes were cut into disks with a diameter of 10 mm. The typical mass loading of active materials on the cathode is 5 mg cm^{-2}. The capacity ratio of negative electrode capacity/positive electrode capacity (N/P ratio) for LCO||graphite pouch cells is 1.07: 1, and the mass loadings of the graphite anode and the LCO cathode for pouch cells are 10.2 and 16.2 mg cm^{-2}, respectively. The EC electrolyte (baseline electrolyte) is composed of 1.0 M $LiPF_6$ in EC/EMC (3:7, by volume ratio), the EC-DEC electrolyte is composed of 1.0 M $LiPF_6$ in EC/EMC/DEC (3:4:3), the FEC electrolyte is composed of 1.0 M $LiPF_6$ in FEC/EMC/DEC (3:4:3), the FEC-DFEC electrolyte is composed of 1.0 M $LiPF_6$ in FEC/DFEC/EMC/DEC (1.5:1.5:4:3), the DFEC electrolyte is composed of 1.0 M $LiPF_6$ in DFEC/EMC/DEC (3:4:3). The coin-type (CR2032) LCO||Li half-cells were assembled with LCO cathode, lithium metal, Celgard film and 60 μL electrolyte in an Ar-filled glove box. The LCO||graphite pouch cells were assembled in the pouch-cell production line and each pouch cell was filled with 6 g of the electrolyte.

Electrochemical Measurement

The galvanostatic electrochemical measurements were carried out in the NEWARE battery test system at 25 °C. To analyze the long-term cyclability, the coin cells were charged and discharged at 0.2 C (1 C = 200 mA g^{-1}) for three cycles, and charged and discharged at the same current for the long-term cycles within the voltage range of 3.0-4.6 V. The linear sweep voltammetry (LSV) and cyclic voltammetry (CV) measurements were performed on the Solartron Analylical 1470E electrochemical workstation at the scanning rate of 0.1 and 0.2 mV s^{-1}, respectively. The *in-situ*/*ex-situ* electrochemical impedance spectroscopy (EIS) was performed on the Solartron Analylical 1470E electrochemical workstation at the frequency range of 1000 kHz-0.01 Hz. The galvanostatic intermittent titration

technique (GITT) was tested in the NEWARE battery test system with the procedure of charging/discharging for 10 min and standing for 30 min.

Materials Characterization

The powder X-ray diffraction (XRD) and *in-situ* XRD measurement were performed on a Bruker D8 Advance diffractometer with a Cu-Kα radiation source. Morphology and elemental distribution investigation of the samples were conducted using a scanning electron microscope (SEM, Zeiss SUPRA-55). The transmission electron microscope (TEM) was collected on a field-emission transmission electron microscope (FETEM, JEOL-3200FS) operating at an accelerating voltage of 300 kV with a 60 cm camera length, a minimum collection angle of -30° to 30°, and a OneView CMOS camera (Gatan Inc.). The focused ion beam (FIB, FEI-Scios) milling were used for the preparation of high-quality thin lamellar samples for TEM studies on the cross-section images of materials. The (cryogenic transmission electron microscopy) cryo-TEM images were collected on JEOL-3200FS microscope, and the observation of the interphase layer for LCO particles after cycles was done in a -172 °C environment by a cryo transfer tomography holder (model 2550, Fischione), without the FIB milling process. ^{7}Li nuclear magnetic resonance (NMR) were recorded on a Quantum-I Plus 400 MHz NMR spectrometer. FTIR spectra were collected on a Nicolet Avatar 360 spectrophotometer (ATR). The electrolyte Raman spectra were acquired using a miniature laser confocal Raman spectrometer (Horiba LabRAM HR800, France) with a 785 nm wavelength laser at room temperature. The *in-situ* Raman measurements were taken by a Renishaw InVia Raman microscope with a 633 nm wavelength laser, CR2032-type coin cell with a small hole covered by a 2 mm thick sapphire were assembled to ensure the irradiation of the LCO surface though Li metal foil and a glass fiber separator. The *in-situ* ultraviolet-visible (UV-Vis) tests were carried out using a quartz cuvette assembled with LCO cathode, Li mental and 2 mL electrolyte on a UV-Vis spectrometer (Shimadzu UV2600). The content of Co dissolution (dissolved Co in electrolyte and deposited Co on Li anode) in *in-situ* UV-Vis test was analyzed using inductively coupled plasma-optical emission spectroscopy (ICP-OES, Horiba Jobinyvon JY2000-2). The chemical states of the selected elements were investigated by X-ray photoelectron spectrometry (XPS) on a Thermo Scientific Escalab 250Xi spectrometer. Time-of-flight secondary ion mass spectrometry (TOF-SIMS) measurements were carried out on a Nano TOF-2

instrument (ULVAC- PHI, Japan) equipped with a Bi^{3+} beam (30 kV) cluster primary-ion gun for analysis and an Ar^{+} beam (3 keV 100 nA) using a sputtering rate of 0.1 nm s^{-1} to obtain the desired depth profile. The area of analysis was 100 × 100 μm^2, whereas the sputtering area was 400 × 400 μm^2. The soft X-ray absorption spectroscopy (sXAS) experiments were carried out in the TEY mode under ultra-high vacuum at the Catalysis and Surface Science Endstation at the BL11U beamline in the National Synchrotron Radiation Laboratory (NSRL) in Hefei, China. The *in-situ* differential electrochemical mass spectrometry (DEMS) experiments utilized ECC-DEMS cell (EL-CELL) and on-line mass spectrometry (HPR-20 EGA).

Theoretical calculations

All the structures were optimized at B3LYP/6-311+G** level of theory using Gaussian 16 program package.[1-3] The implicit solvation model employed in the simulations was the Solvation Model based on Density (SMD) with dimethyl sulfoxide as the solvent.[4] Frequency calculations were performed at the same level to confirm the nature of the stationary structures.

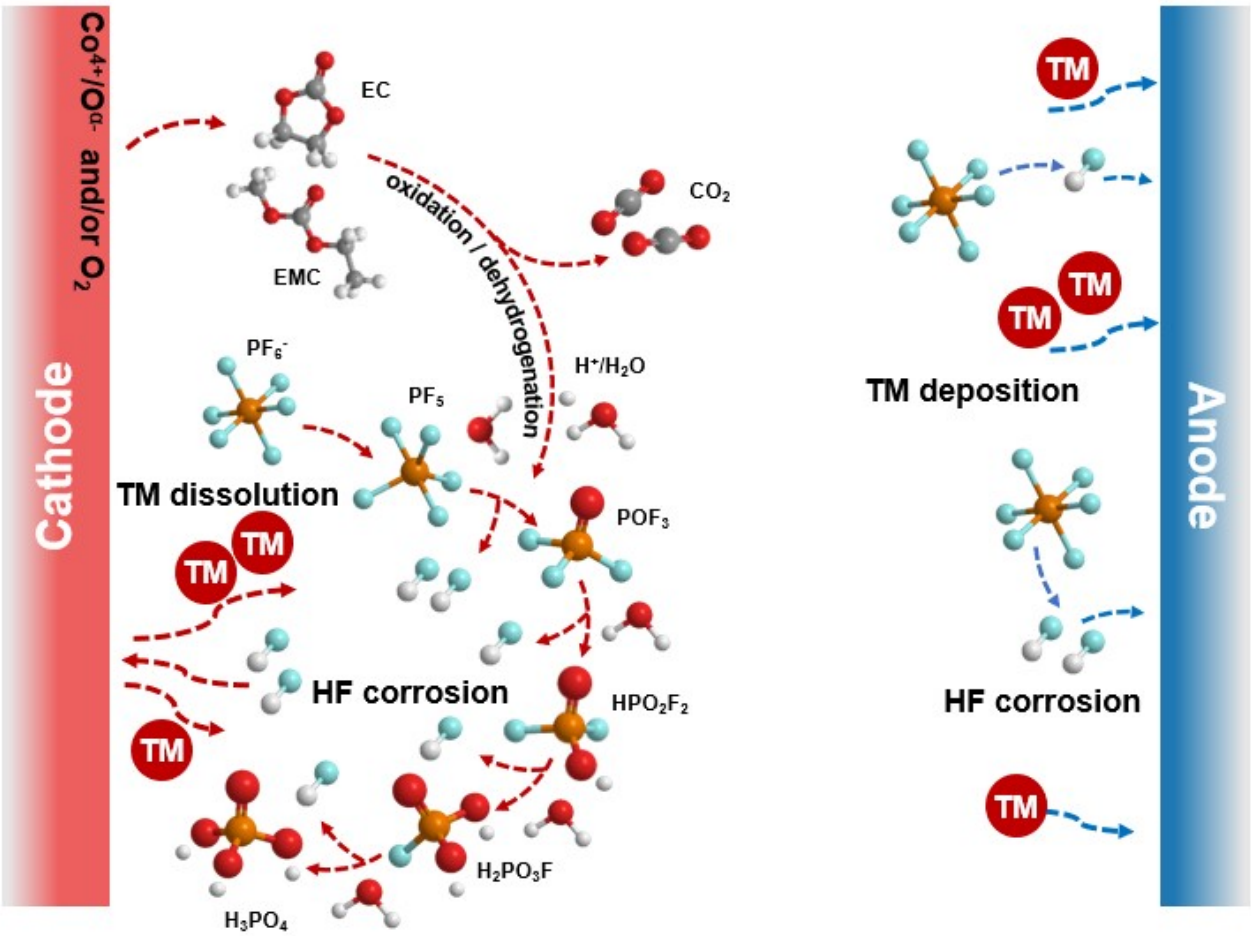

Fig. S1 The schematic diagram of the interfacial side reactions in $LiPF_6$ and EC/EMC based electrolyte at high voltage initiated at cathode material.

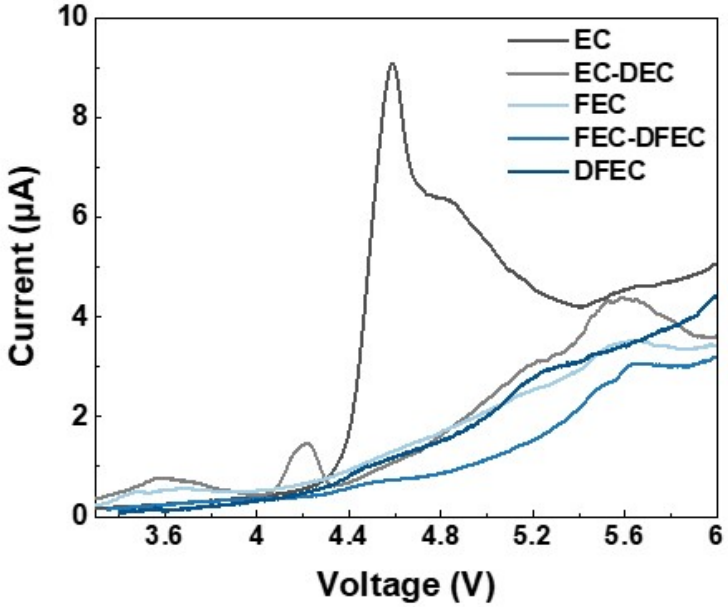

Fig. S2 Oxidation stability of different electrolytes evaluated by linear sweeping voltammetry (LSV) on a stainless steel at a scanning rate of 0.1 mV s^{-1}.

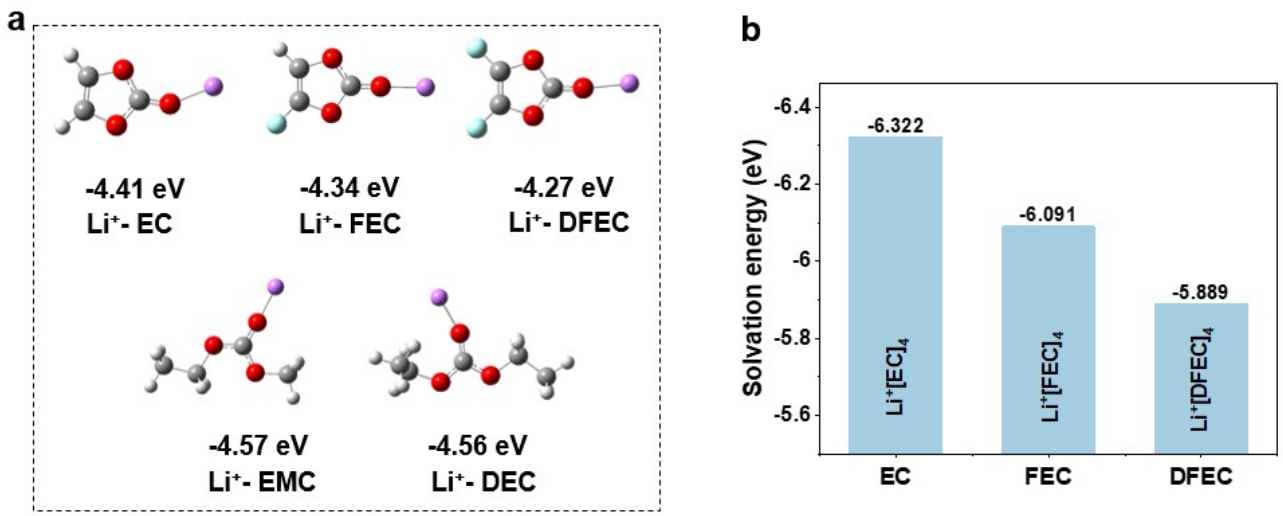

Fig. S3 a) The interaction strength between Li^+ and solvent obtained by first-principles calculations and b) the Calculated the Li^+ ions solvation energy in $Li^+[FEC]_4$, $Li^+[DFEC]_4$ solvation structure. ($\Delta E_{solvation\ energy}=E_{solvation\ structure}-E_{Li+}-E_{solvents}$).

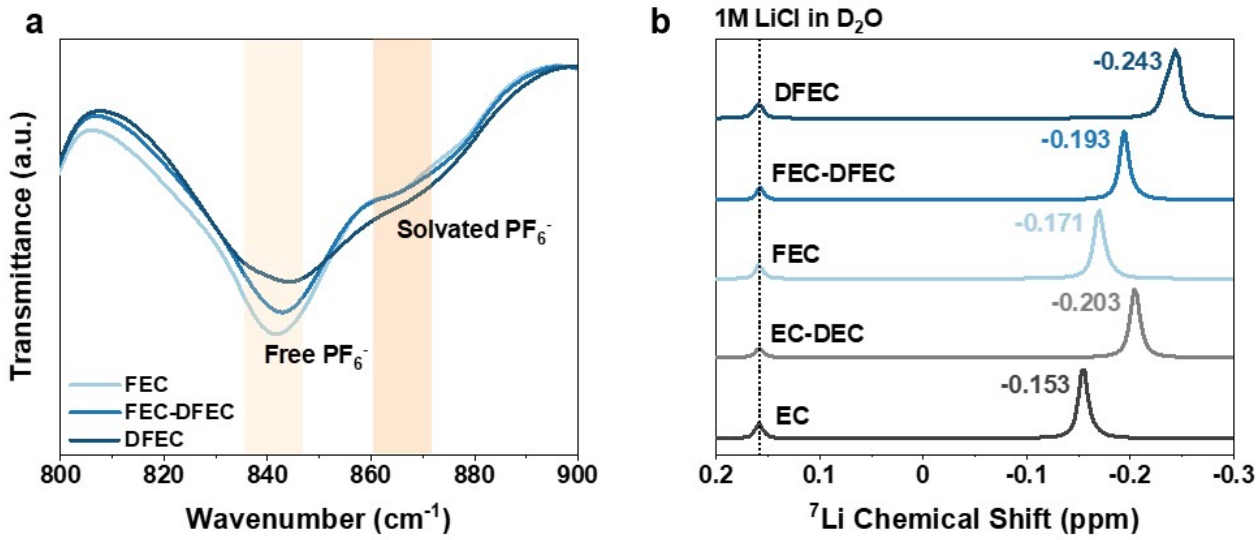

Fig. S4 a) The FTIR spectra of FEC, FEC-DFEC and DFEC electrolytes. b) The ^{7}Li-NMR spectra of different electrolytes. A coaxial internal insert that contains a standard NMR solvent (1M LiCl D_2O) was inserted into the NMR tube to enable analysis while preserving the pristine microstructure of the electrolyte.

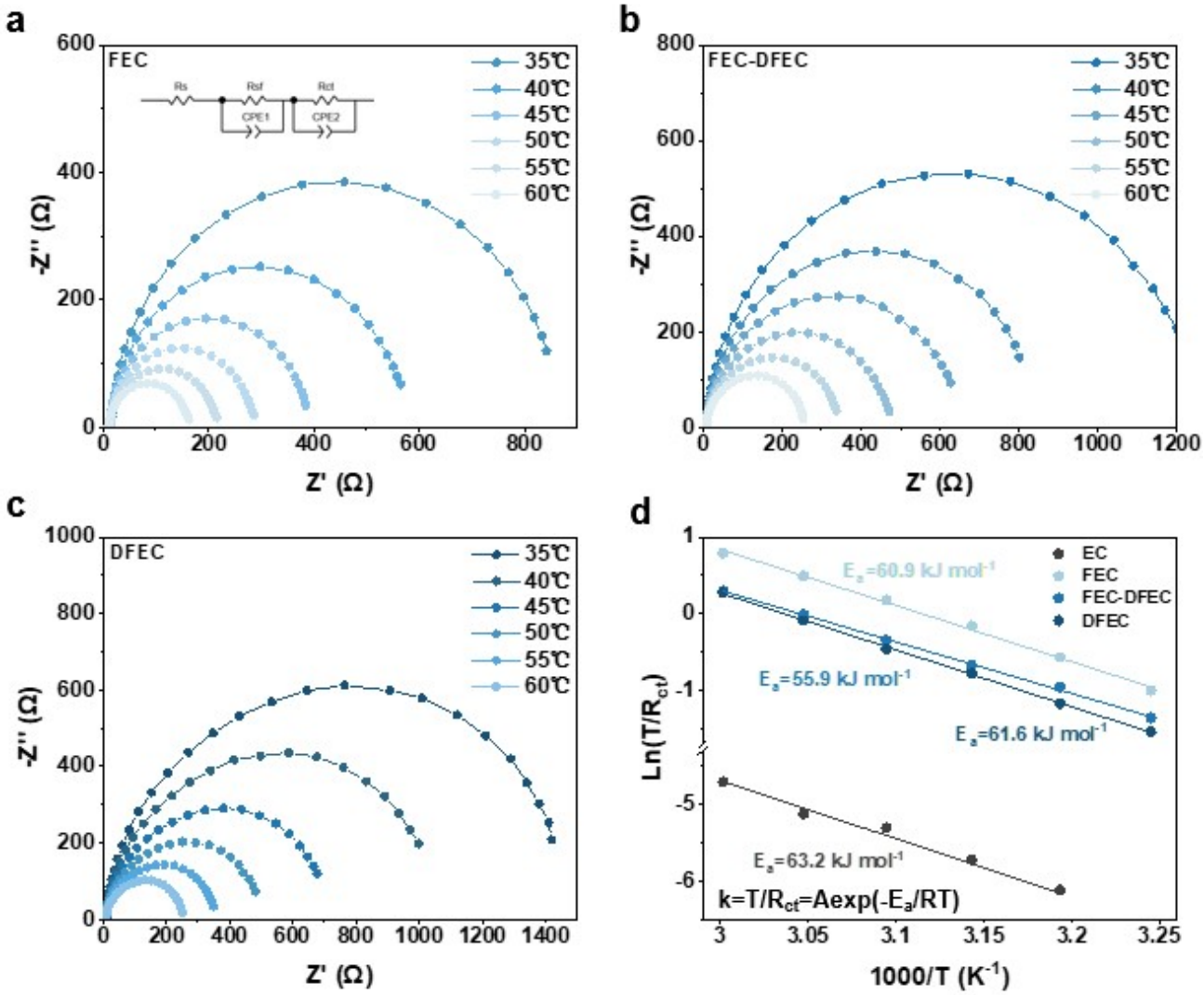

Fig. S5 Nyquist plots for $Li_{0.7}CoO_2$||$Li_{0.7}CoO_2$ symmetric cells at different temperatures (308.15 K to 333.15 K corresponds to 35 to 60 °C) in a) FEC, b) FEC-DFEC and c) DFEC electrolytes. d) Arrhenius behavior of the resistance corresponding to Li^+ desolvation energy (E_a) in different electrolytes. (We first assembled LCO||Li cells, charged at 0.2 C for 2 h and disassembled the cells to obtain the $Li_{0.7}CoO_2$ cathode electrodes, then we used two $Li_{0.7}CoO_2$ cathode electrodes to assemble $Li_{0.7}CoO_2$||$Li_{0.7}CoO_2$ symmetric cell).

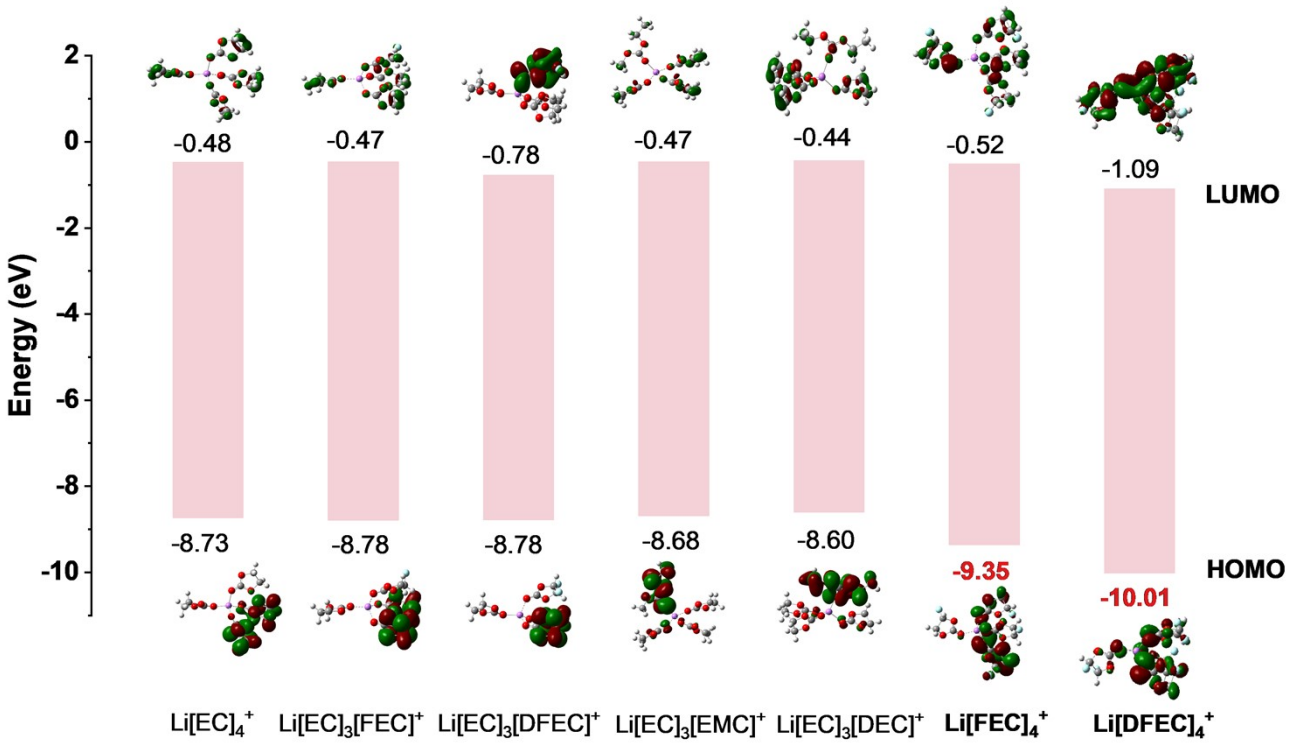

Fig. S6 Calculated HOMO/LUMO energy of various Li^{+}[solvents]$_4$ solvation structure.

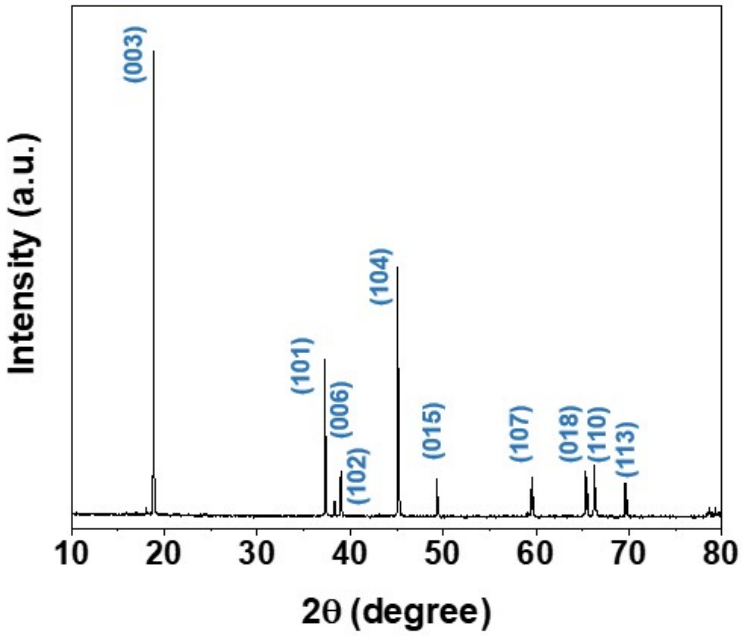

Fig. S7 The XRD diffraction of LCO powders.

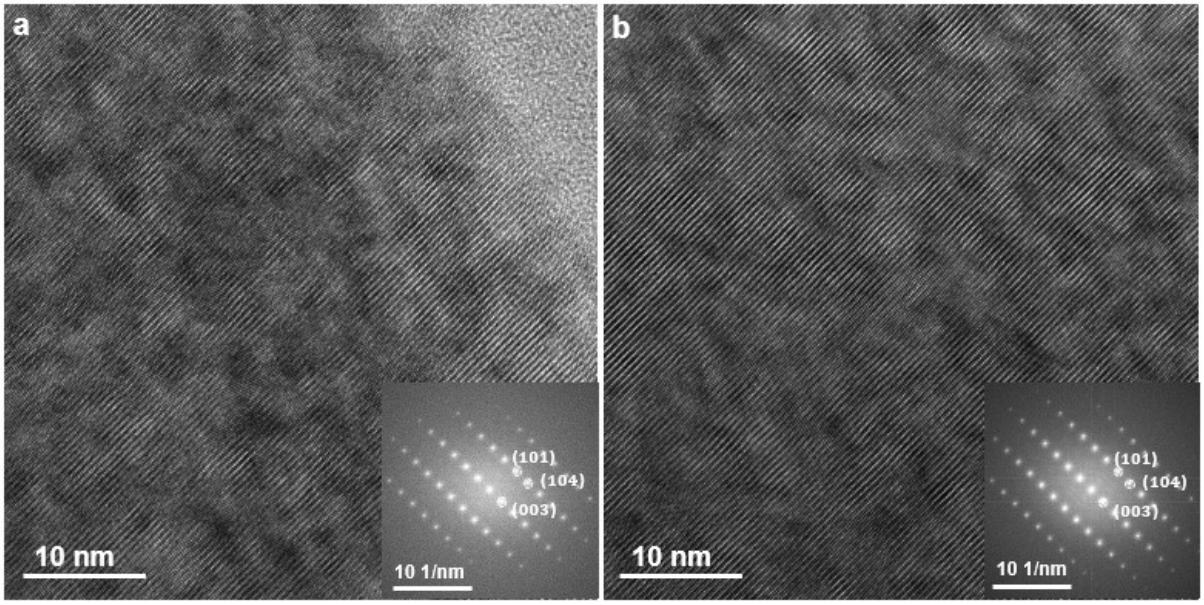

Fig. S8 High-resolution TEM images of the a) surface and b) bulk region of pristine LCO and the corresponding fast Fourier transform (FFT) image.

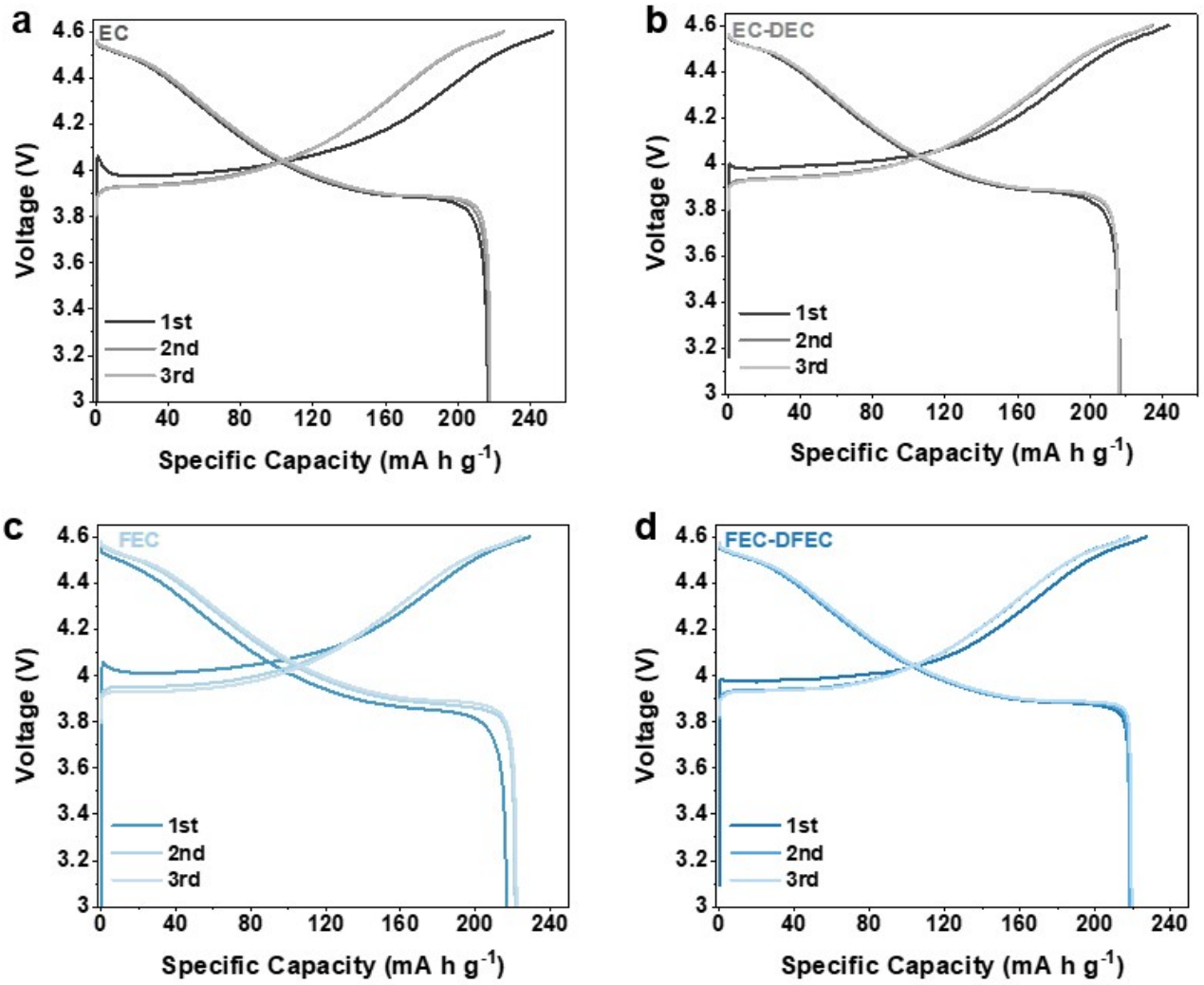

Fig. S9 Charge and discharge curves of LCO||Li half cells within a voltage range of 3.0-4.6 V at 0.2 C for the initial three cycles in a) EC, b) EC-DEC, c) FEC and d) FEC-DFEC electrolytes.

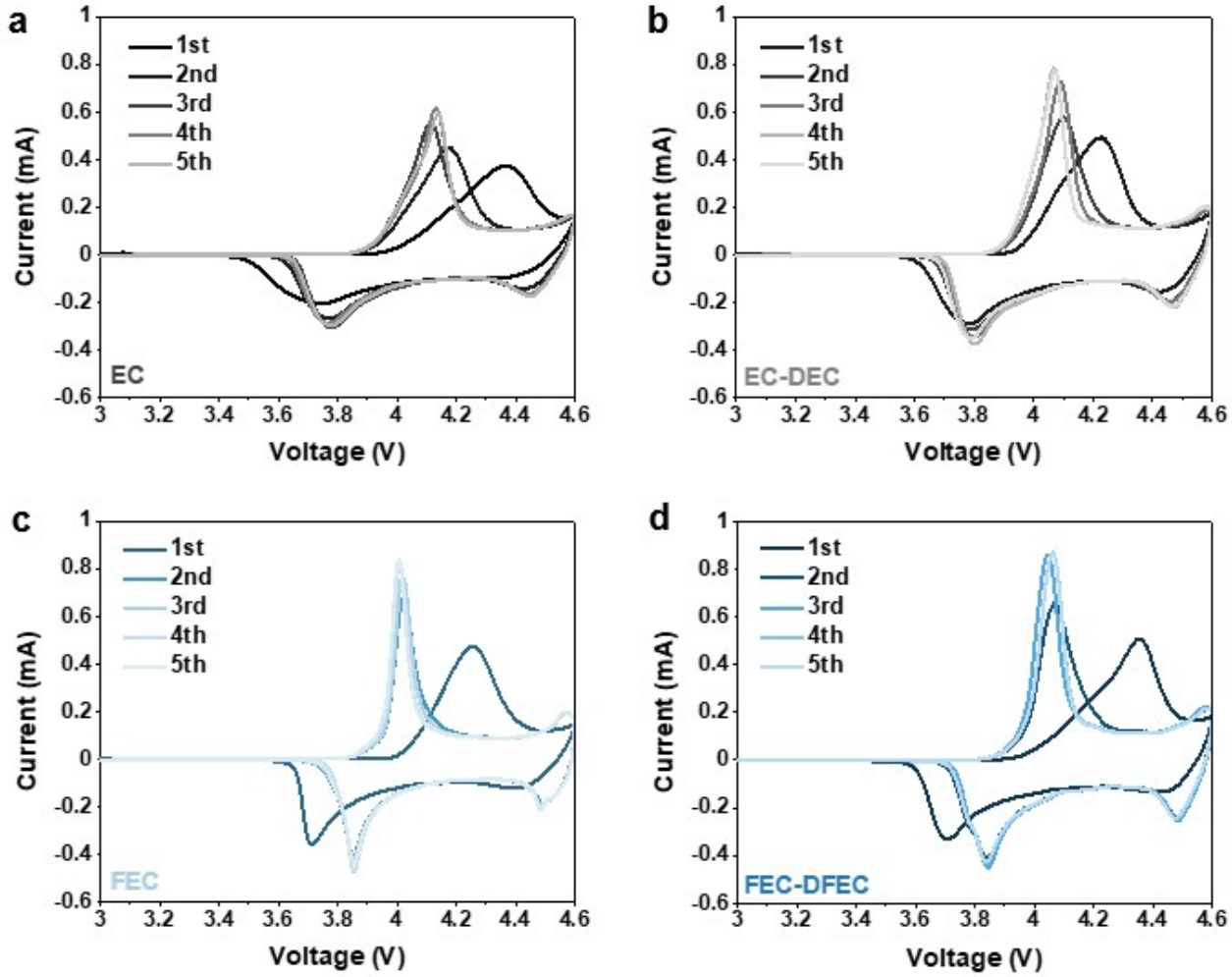

Fig. S10 CV curves of LCO||Li half cells within a voltage range of 3.0-4.6 V at the scanning rate of 0.2 mV s^{-1} in a) EC, b) EC-DEC, c) FEC and d) FEC-DFEC electrolytes.(The CV curves in Fig. 2b are the third cycle of Fig. S10)

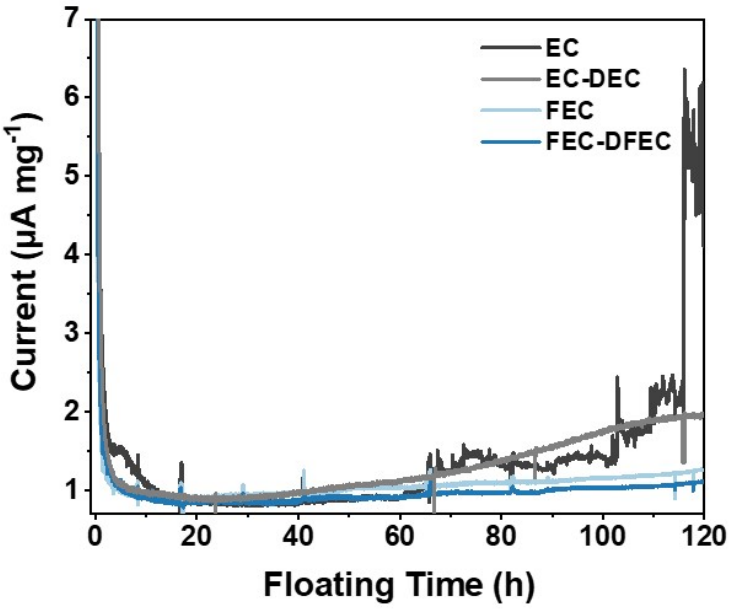

Fig. S11 Leakage current at a 4.6 V constant-voltage floating test of LCO||Li cells in different electrolytes at 45°C.

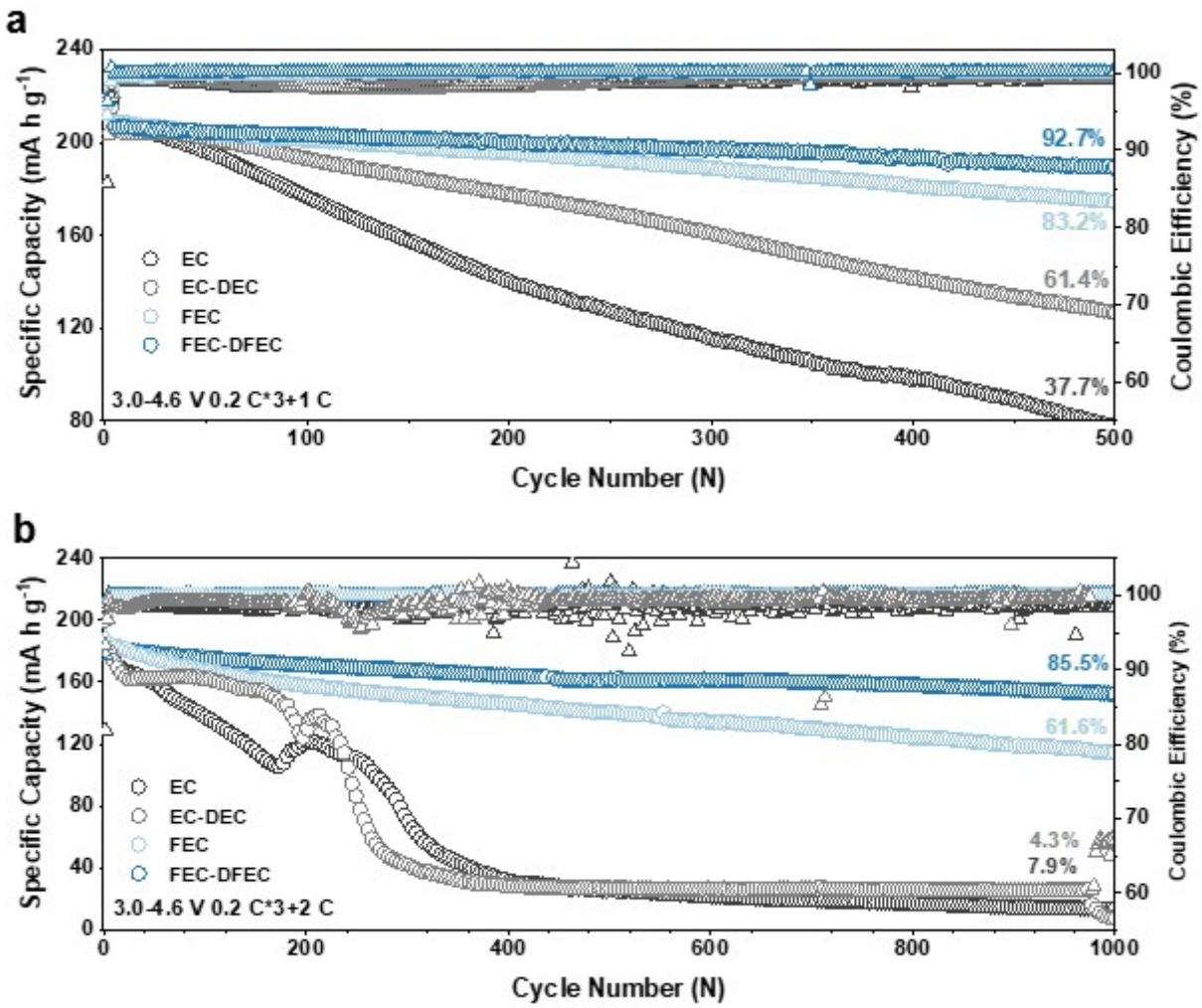

Fig. S12 Cycling performance of LCO||Li half cells in different electrolytes within a voltage range of 3.0-4.6 V at a) 1 C and b) 2 C.

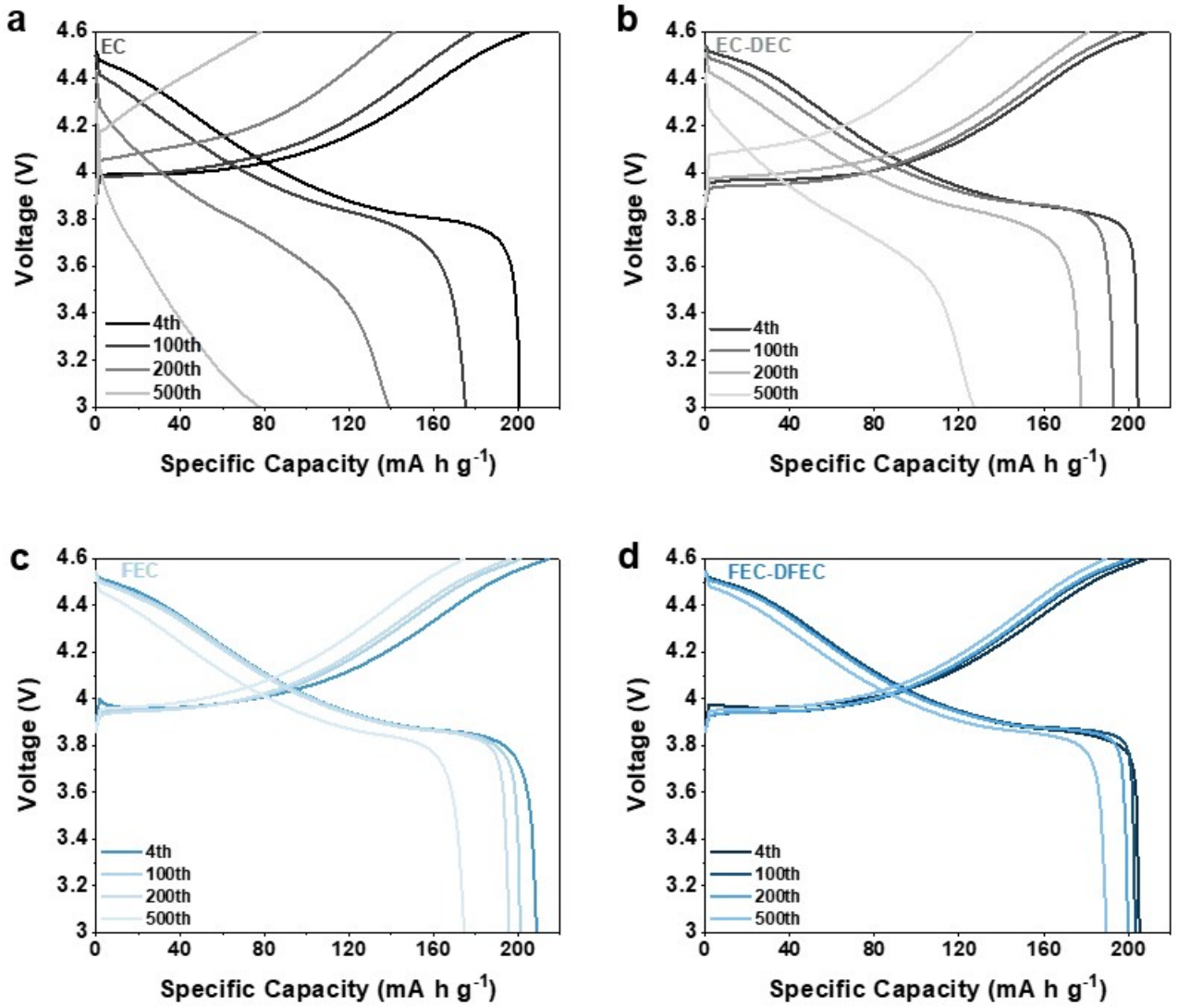

Fig. S13 Charge and discharge curves of LCO||Li half cells within a voltage range of 3.0-4.6 V at 1 C in a) EC, b) EC-DEC, c) FEC and d) FEC-DFEC electrolytes.

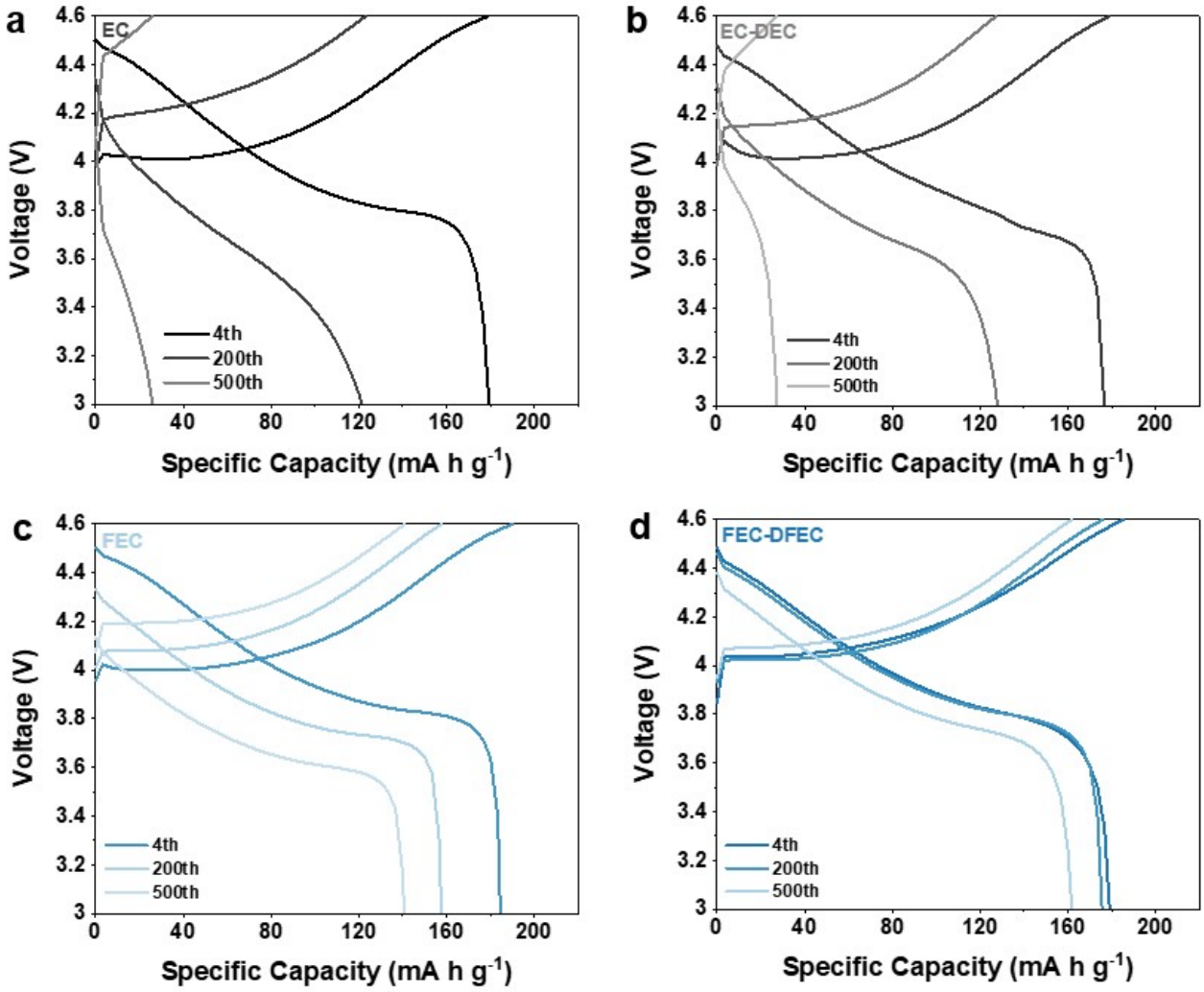

Fig. S14 Charge and discharge curves of LCO||Li half cells within a voltage range of 3.0-4.6 V at 2 C in a) EC, b) EC-DEC, c) FEC and d) FEC-DFEC electrolytes.

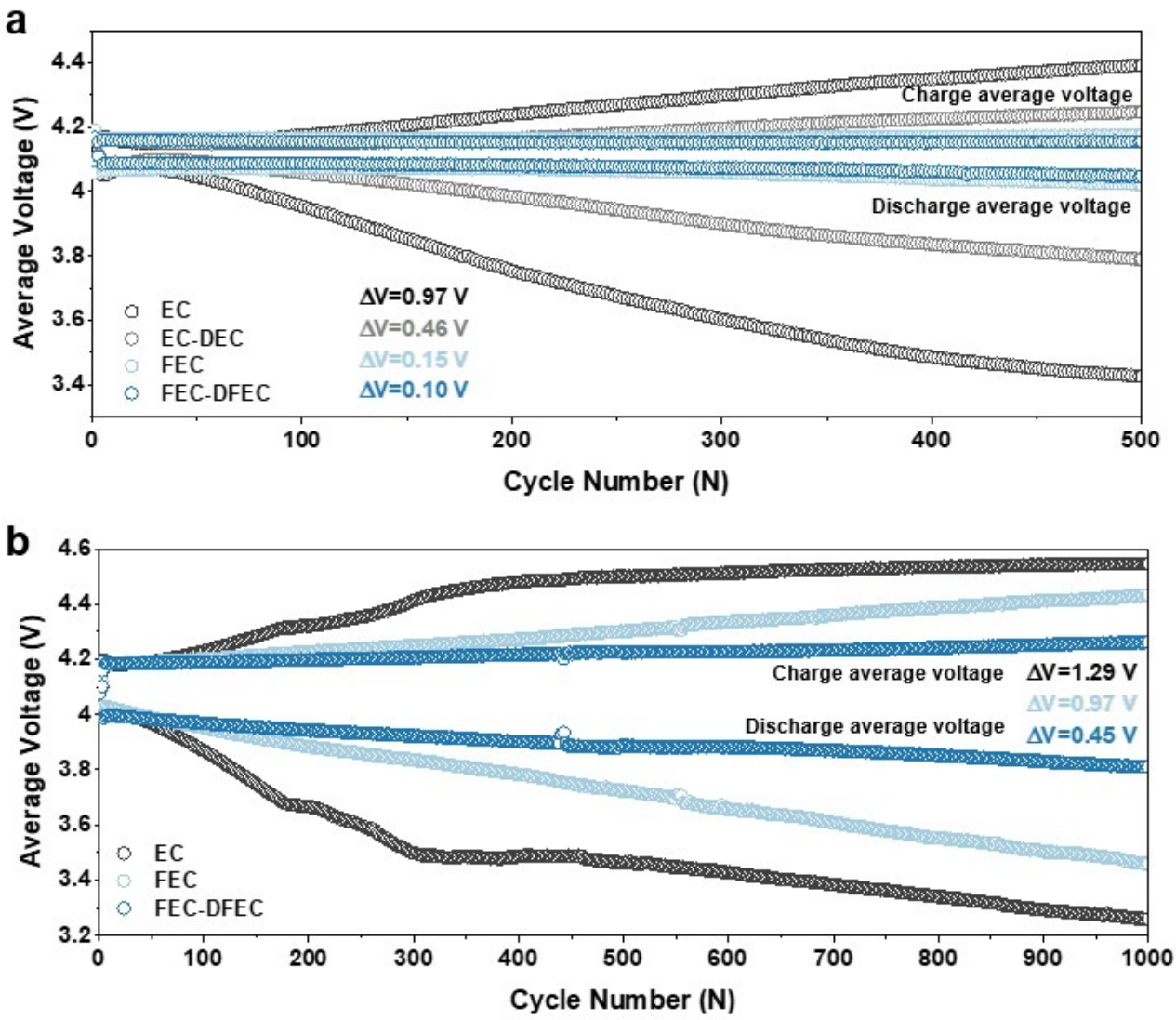

Fig. S15 The changing process of the charge and discharge average voltage upon cycling of LCO||Li half cells in different electrolytes within a voltage range of 3.0-4.6 V at a) 1 C and b) 2 C.

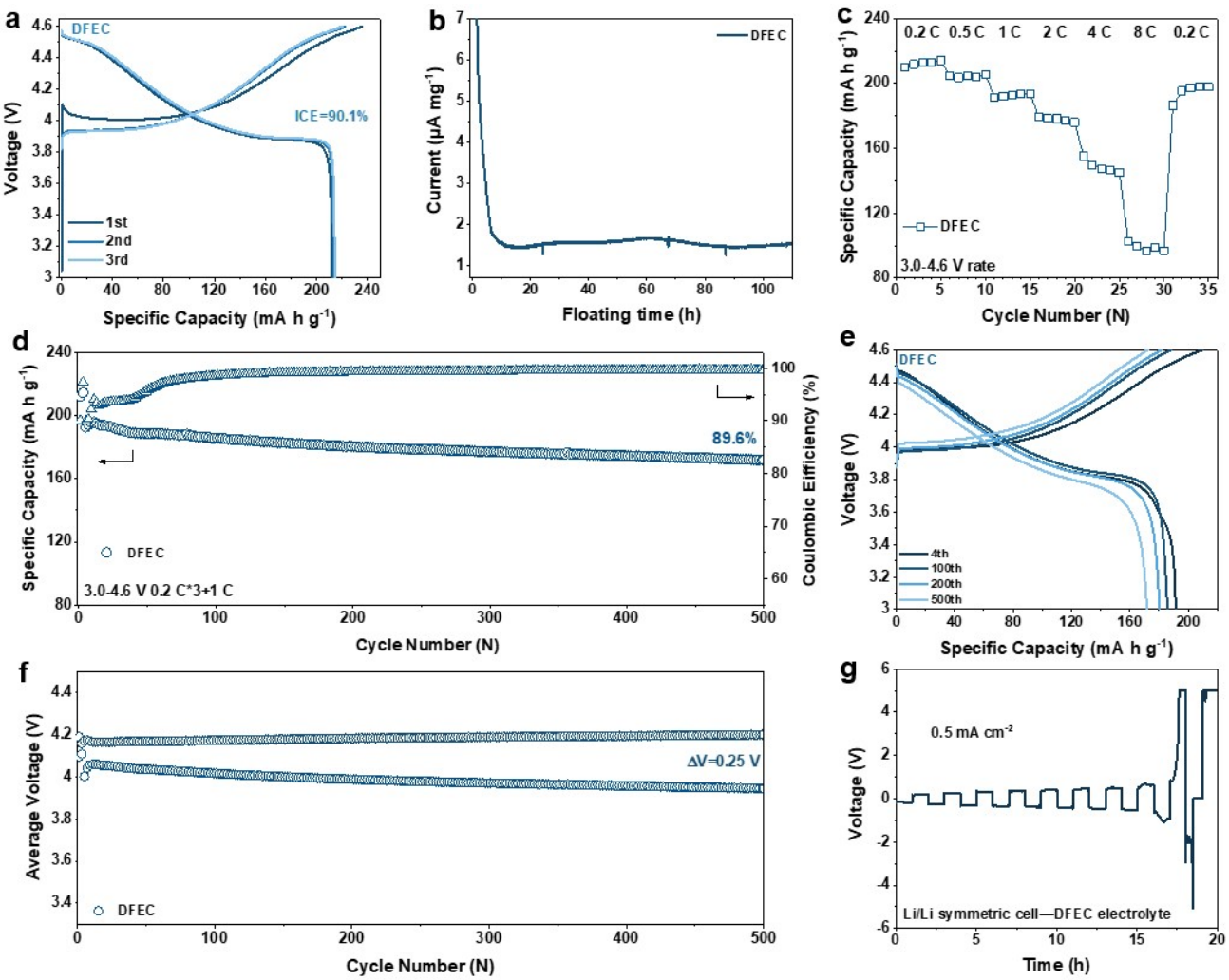

Fig. S16 a) Charge and discharge curves of LCO||Li half cells in DFEC electrolyte within a voltage range of 3.0-4.6 V at 0.2 C for the initial three cycles. b) Leakage current at a 4.6 V constant-voltage floating test of LCO||Li cells in DFEC electrolytes at 45°C. c) Rate performance of LCO||Li half cells in DFEC electrolytes within a voltage range of 3.0-4.6 V. d) Cycling performance of LCO||Li half cells in DFEC electrolyte within a voltage range of 3.0-4.6 V at 1 C, e) the corresponding charge and discharge curves in different cycles, and f) the changing process of the charge and discharge average voltage upon cycling. g) Cycling stability of Li||Li symmetric cells in DFEC electrolyte.

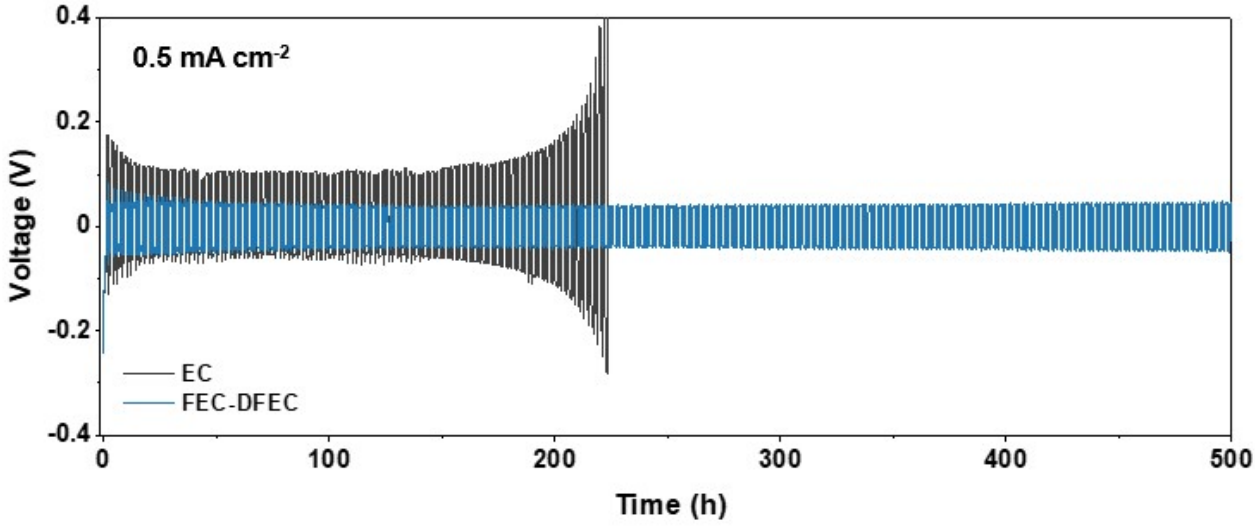

Fig. S17 Cycling stability of Li||Li symmetric cells in different electrolytes.

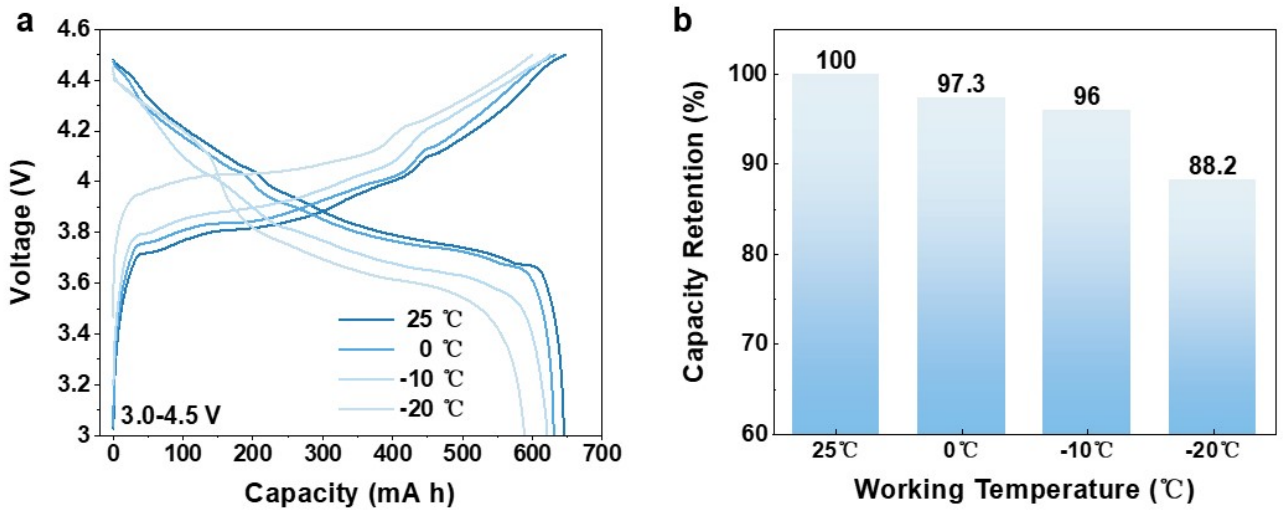

Fig. S18 a) The charge and discharge curves of LCO||graphite pouch cell (0.1 A h) within a voltage range of 3.0-4.5 V at 0.15 C in FEC-DFEC electrolytes at 25 ℃, 0 ℃, -10 ℃ and -20 ℃. b) The corresponding capacity retention of LCO||graphite pouch cell at different temperatures. (0.1 A h pouch cell use the commercial LCO without 4000 ppm Al doping)

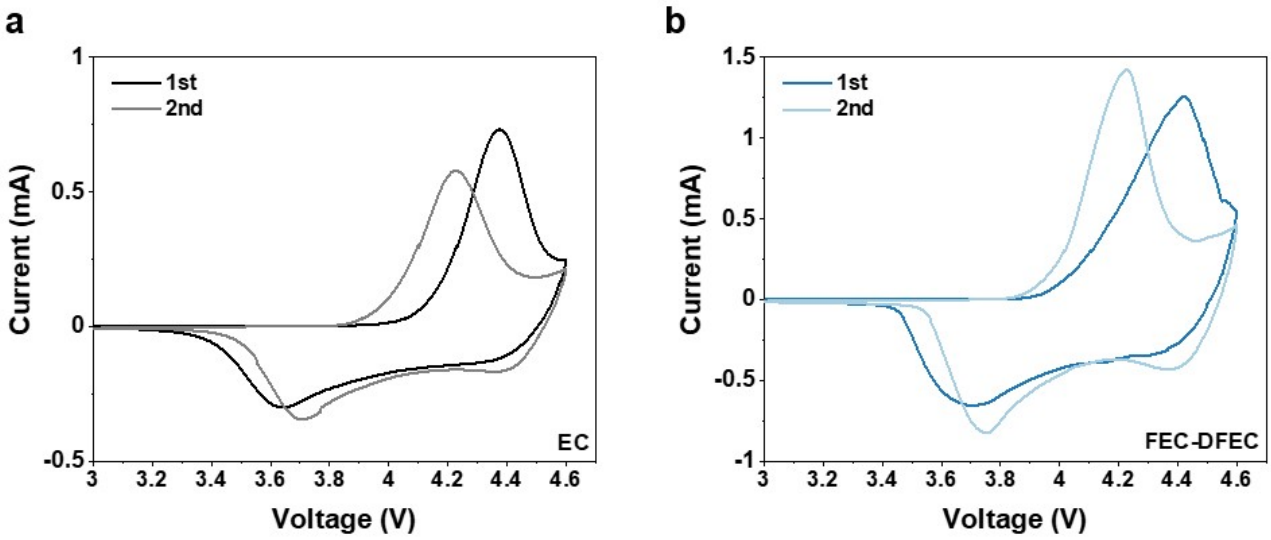

Fig. S19 The CV curves of LCO||Li half cells within a voltage range of 3.0-4.6 V at the scanning rate of 0.1 mV s^{-1} in a) EC and b) FEC-DFEC electrolytes in the *in situ* Raman characterizations.

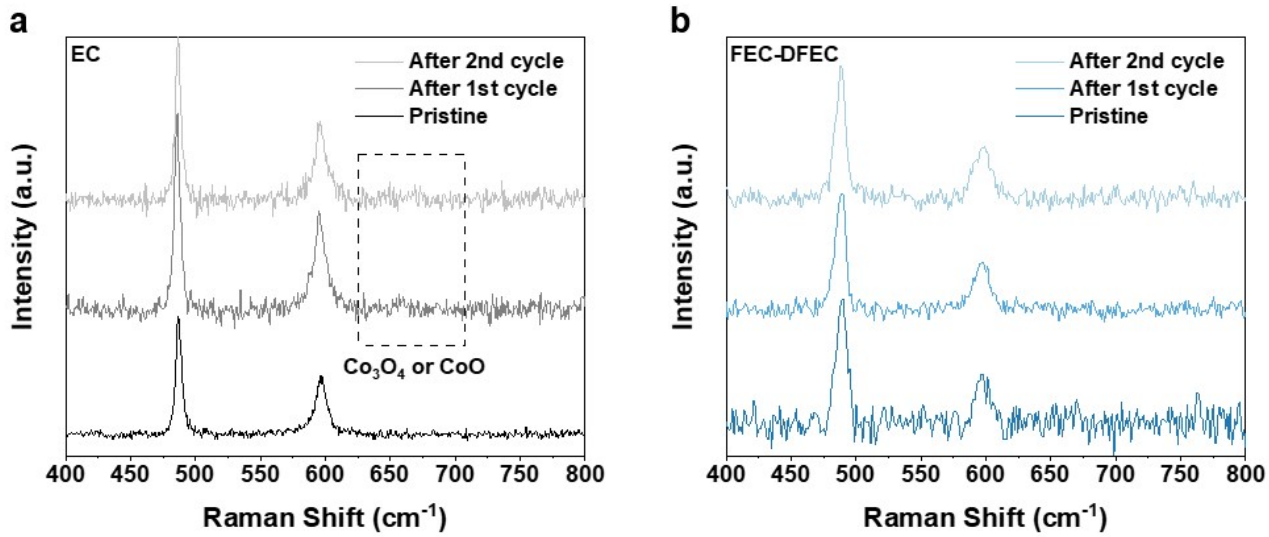

Fig. S20 The Raman spectra of LCO at 3.0 V after first and second cycle during the *in-situ* Raman measurements in a) EC and b) FEC-DFEC electrolytes.

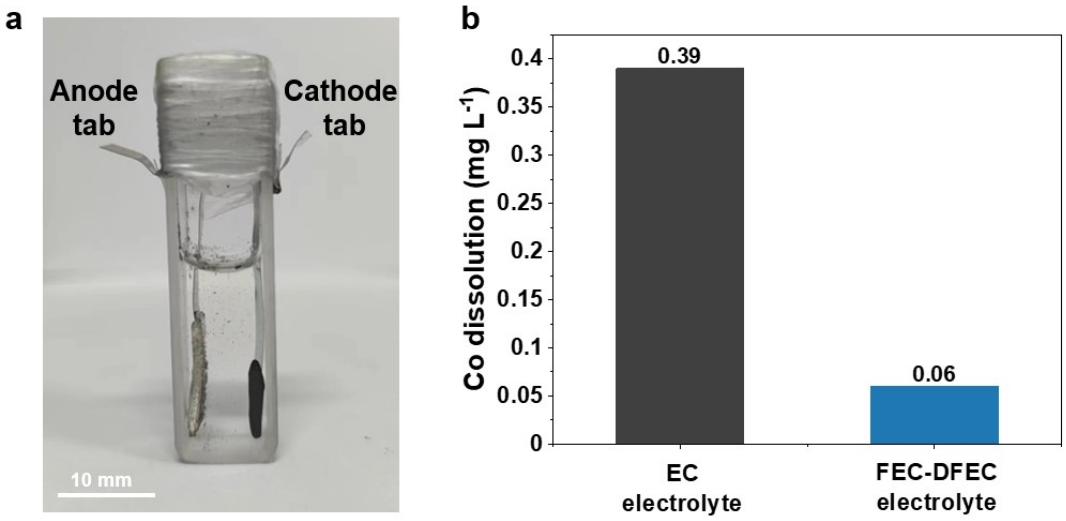

Fig.S21 a) The cell for *in-situ* UV-Vis tests. b) The relative content of Co dissolution after one cycle in UV-Vis tests within a voltage range of 3.0-4.6 V in EC and FEC-DFEC electrolyte.

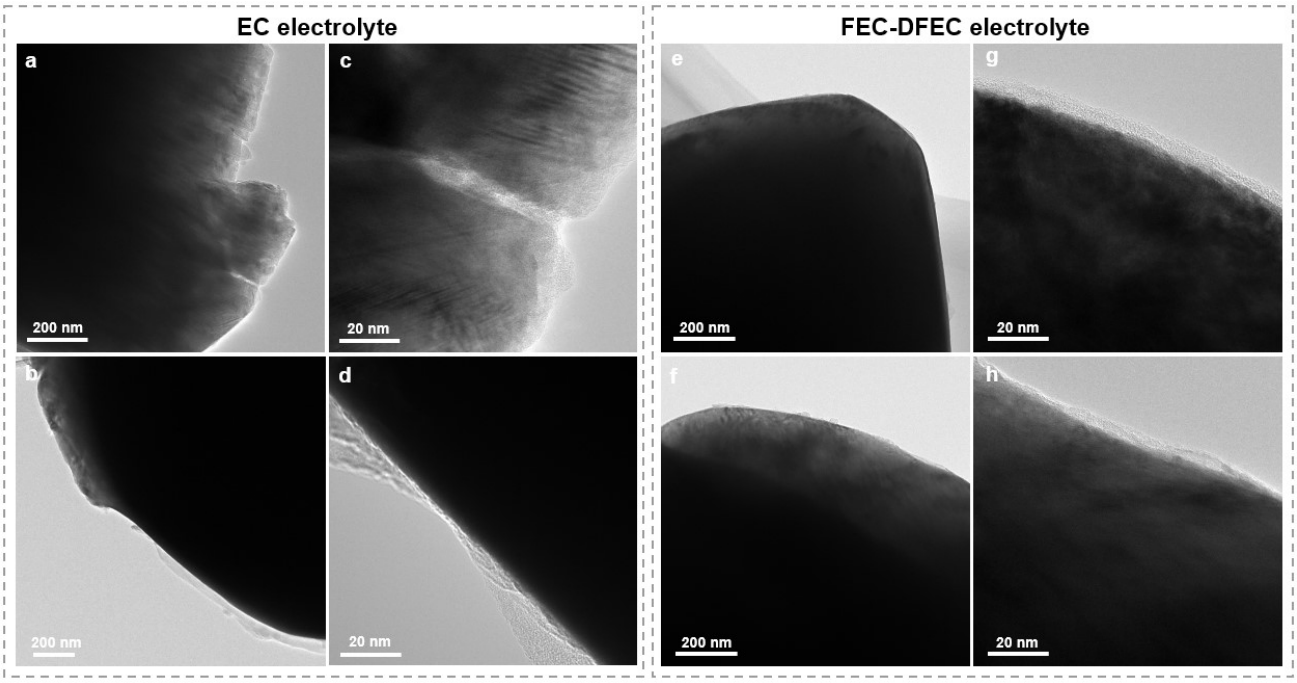

Fig. S22 a,b) The cryo-TEM images of LCO after 10 cycles of LCO||Li cells within a voltage range of 3.0-4.6 V at 1 C in EC electrolyte, c,d) and corresponding enlarged images. e,f) The cryo-TEM images of LCO after 10 cycles of LCO||Li cells within a voltage range of 3.0-4.6 V at 1 C in FEC-DFEC electrolyte, g,h) and corresponding enlarged images.

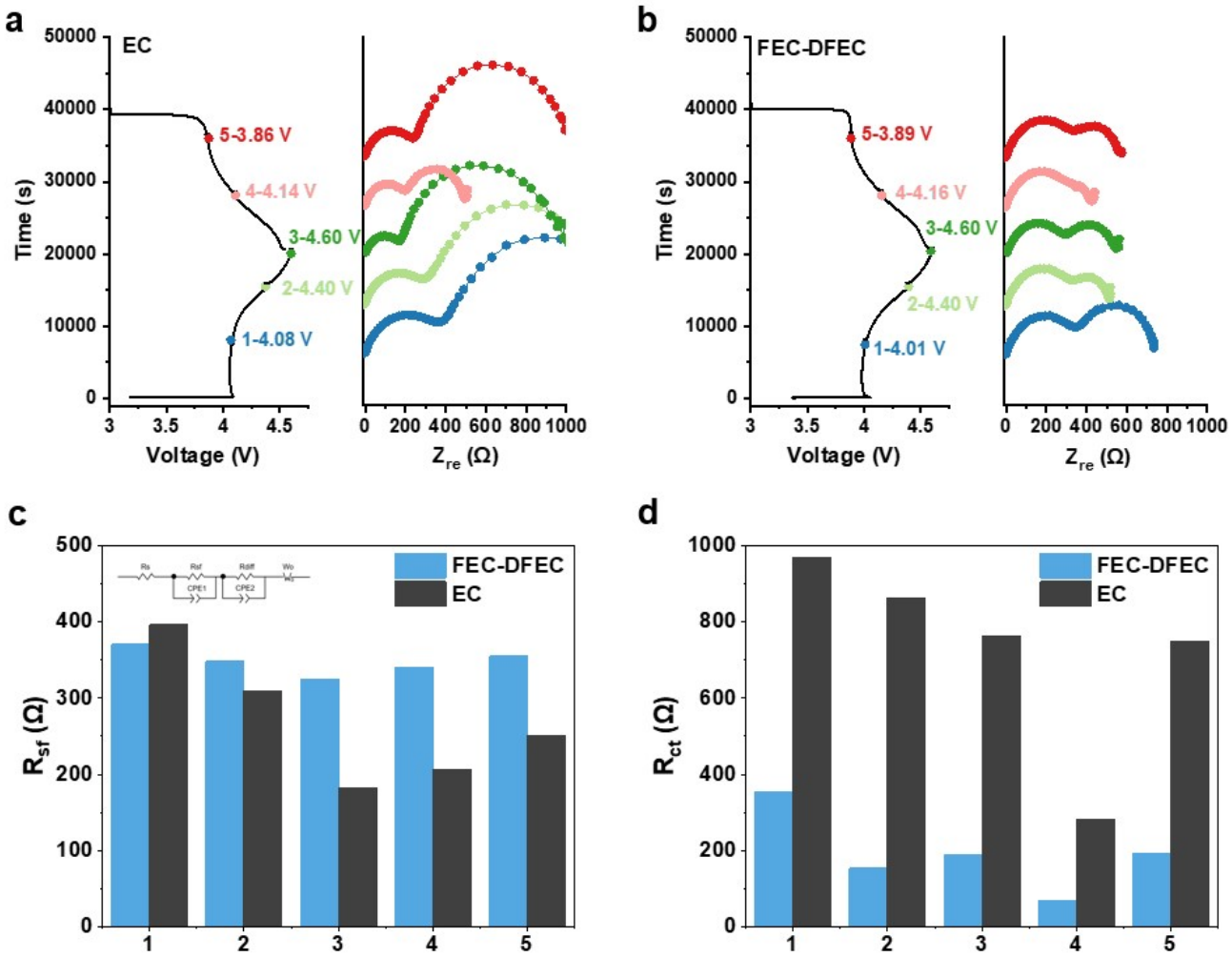

Fig. S23 The *in-situ* EIS measurements of LCO||Li half cells after 10 cycles within a voltage range of 3.0-4.6 V at 1 C in a) EC and b) FEC-DFEC electrolytes. The corresponding fitting results of c) R_{sf} and d) R_{ct} by equivalent circuit.

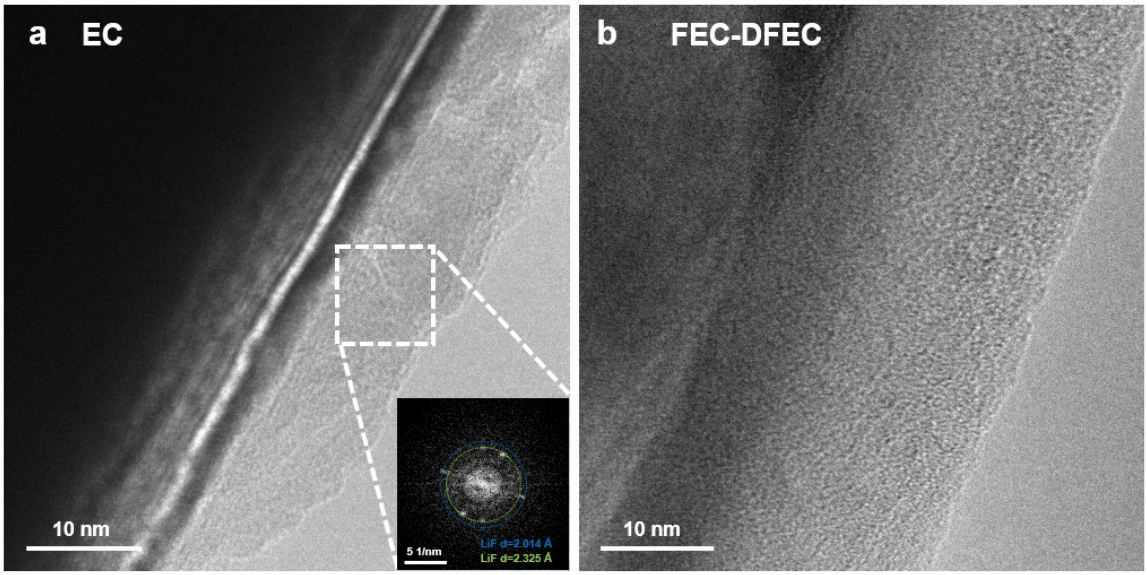

Fig. S24 The cryo-TEM images of LCO CEI layer after 100 cycles of LCO||Li half cells within a voltage range of 3.0-4.6 V at 1 C in a) EC and b) FEC-DFEC electrolytes.

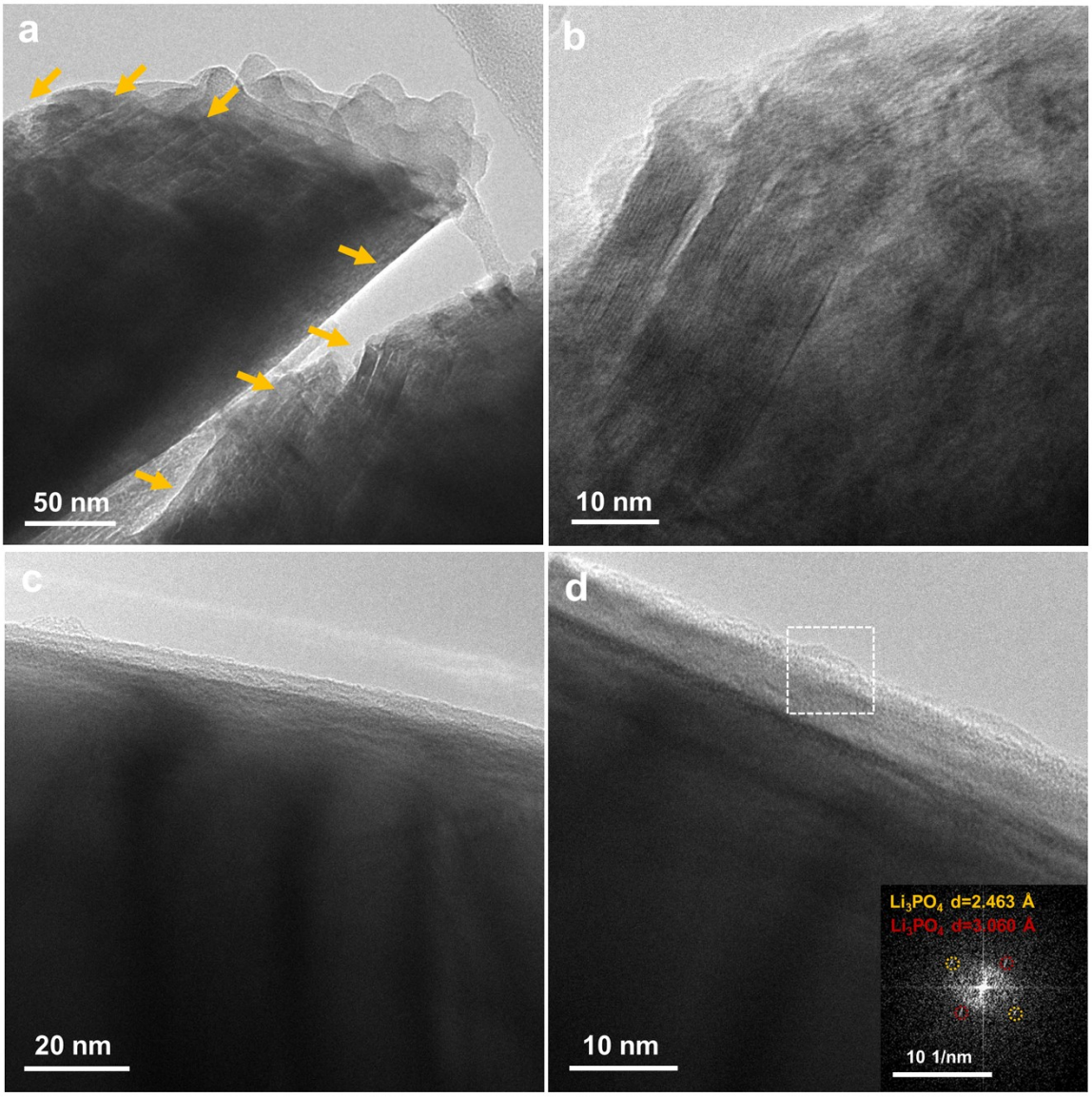

Fig. S25 a) The cryo-TEM images of different LCO particle after 100 cycles of LCO||Li cells within a voltage range of 3.0-4.6 V at 1 C in EC electrolyte, b) and corresponding enlarged images. c) The cryo-TEM images of different LCO particle after 100 cycles of LCO||Li cells within a voltage range of 3.0-4.6 V at 1 C in FEC-DFEC electrolyte, d) and corresponding enlarged images.

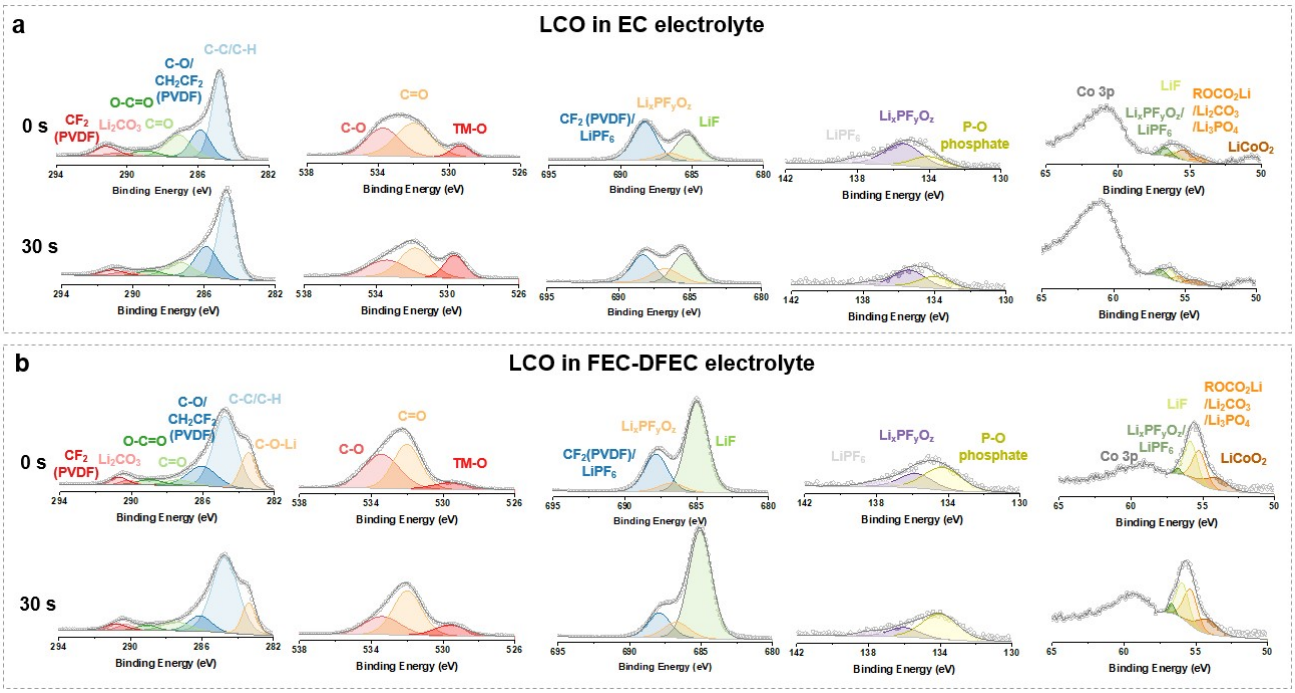

Fig. S26 The C 1s, O 1s, F 1s, P 2p and Li 1s XPS spectra of the LCO cathode electrode with different etching time after 100 cycles of LCO||Li half cells within a voltage range of 3.0-4.6 V at 1 C in a) EC and b) FEC-DFEC electrolytes.

In **Fig. S26**, the analyses of C 1s, O 1s, F1s, P 2p, and Li 1s XPS peaks are as follows,[5]
First, the C 1s peaks can be divided into several peaks, including the C-O, C=O, O-C=O, and Li_2CO_3, locating at the binding energies of 286.2 eV, 287.6 eV, 288.9 eV and 290.3 eV, respectively, which is closely related to the decomposition of solvents. An additional peak, locating at the binding energy of 283.5 eV, can be clearly observed in FEC-DFEC electrolyte, which can be indexed to the C-O-Li organic species from FEC/DFEC decomposition. Second, the O 1s peaks can be separated into three main peaks, including the lattice O, C-O and C=O, locating at 529.8 eV, 532.0 eV and 533.5 eV, respectively. In FEC-DFEC electrolyte, the intensity of lattice O peak is obviously lower than that in EC based electrolyte, mainly due to the homogeneous and thick CEI. Third, for F 1s spectra, the formation of LiF and $Li_xPO_yF_z$, locating binding energy of 685.0 and 686.7 eV, respectively, are mainly attributed to the decomposition of the $LiPF_6$. In FEC-DFEC electrolyte, due to more PF_6^- ions participating in the solvation structure, the intensity of LiF peak is much higher than in EC base electrolyte. Fourth, for P 2p peaks, the peaks representing the phosphate species (i.e. Li_3PO_4, $OP(OR)_3$) and $Li_xPO_yF_z$ + $OPF_x(OR)_y$, locating at binding energies of 134.0 and 135.7 eV, respectively, can further reflect the reaction product of $LiPF_6$, indicating that more phosphate species can be produced in the FEC-DFEC electrolyte. Fifth, for Li 1s peaks, it is noted that, more LiF and $ROCO_2Li$, Li_3PO_4 species exist in the FEC-DFEC electrolyte, locating at binding energies of 56.0 and 55.4 eV, respectively.

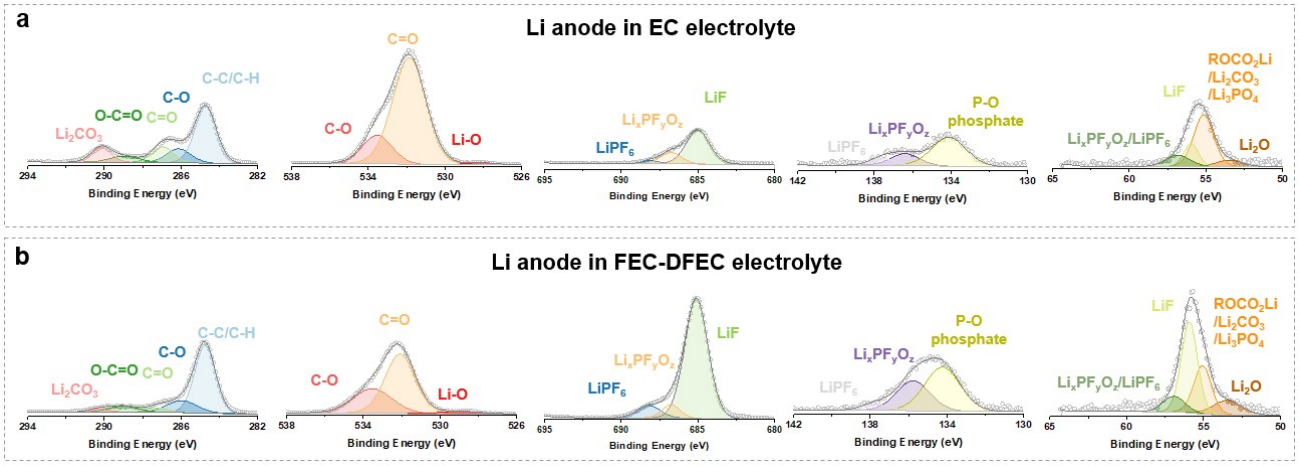

Fig. S27 The C 1s, O 1s, F 1s, P 2p and Li 1s XPS spectra of the Li metal surface after 100 cycles of LCO||Li half cells within a voltage range of 3.0-4.6 V at 1 C in a) EC and b) FEC-DFEC electrolytes.

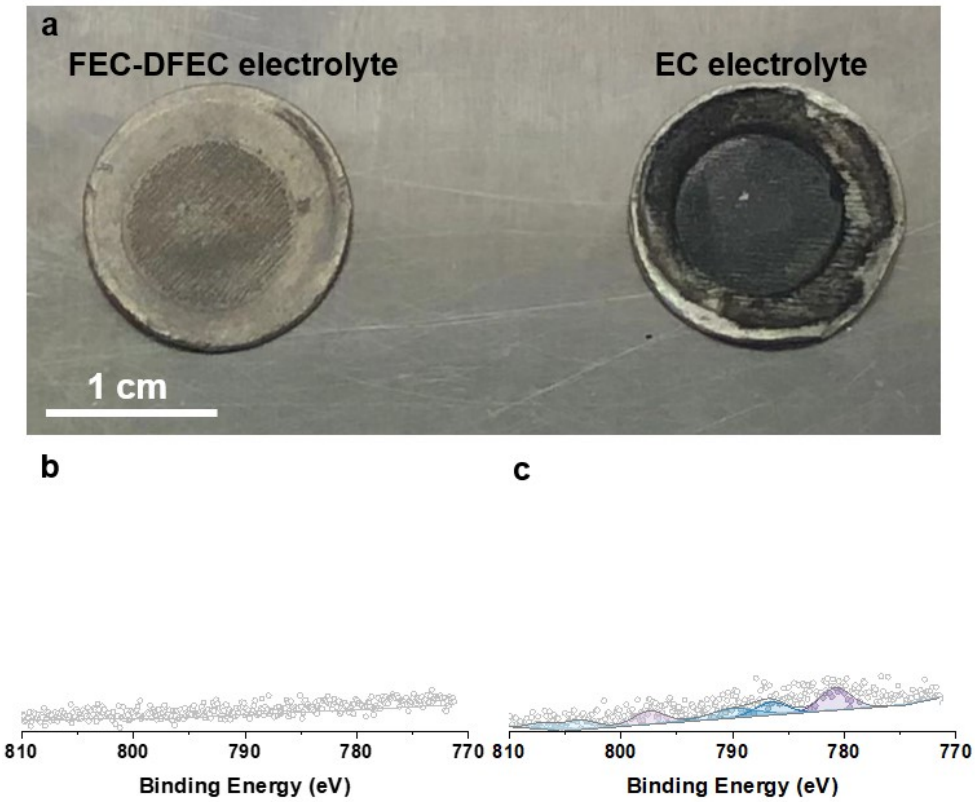

Fig. S28 a) Digital photograph of Li metal after 100 cycles of LCO||Li half cells within a voltage range of 3.0-4.6 V at 1 C in a) EC and b) FEC-DFEC electrolytes. Comparison of Co dissolution situation of b) EC and c) FEC-DFEC electrolytes after 100 cycles by XPS measurements.

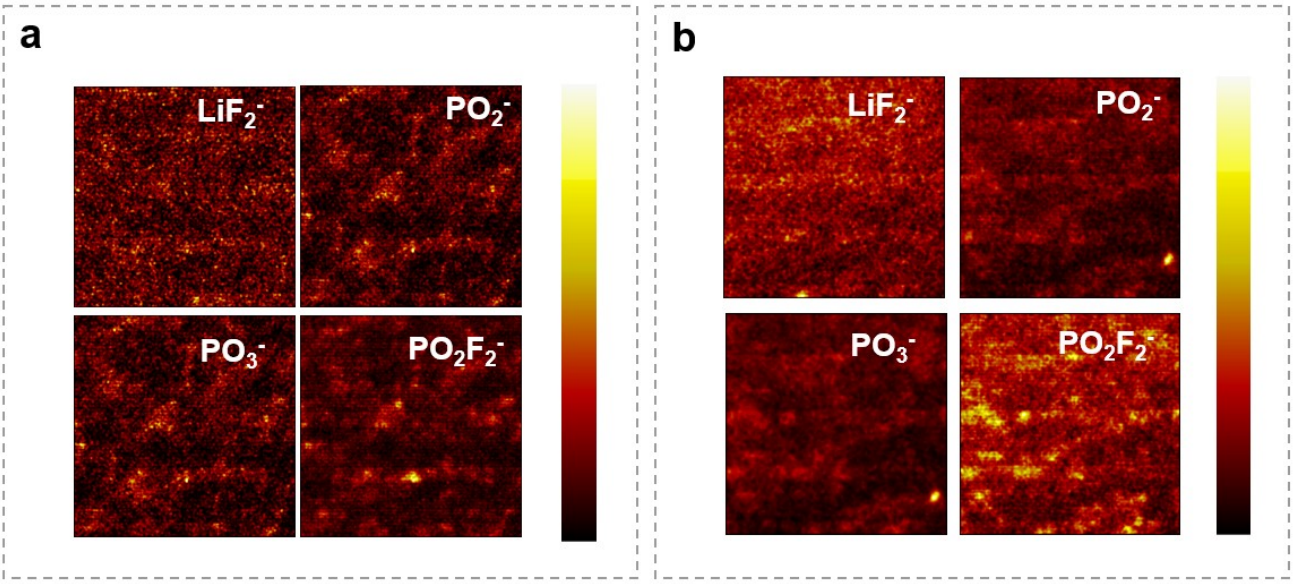

Fig. S29 Top view of TOF-SIMS data for diverse kinds of secondary-ion fragments for the LCO cathode electrolyte interface after 100 cycles in a) EC and b) FEC-DFEC electrolytes.

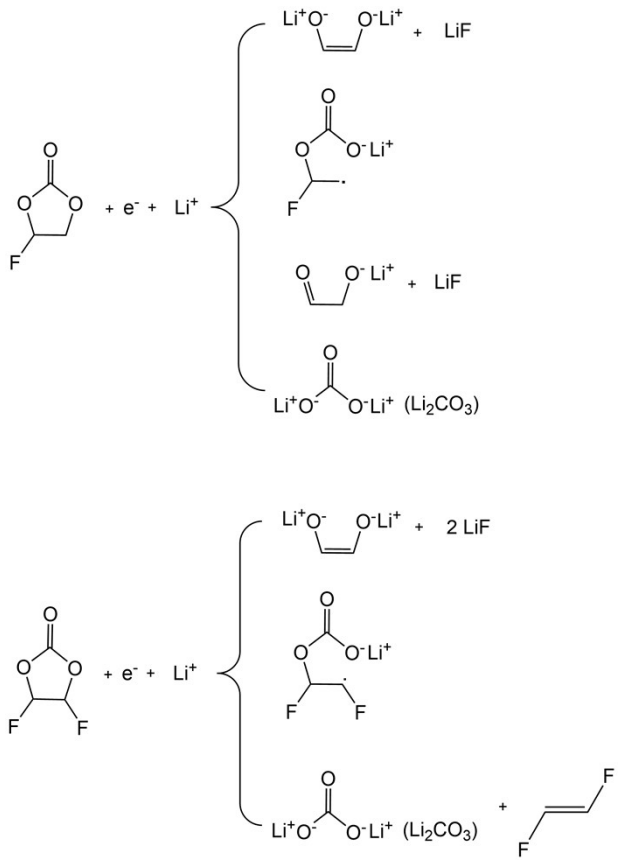

Fig. S30 The possible reduction pathway of FEC and DFEC on the anode side that lead to the lithium alkyl carbonates ($ROCO_2Li$), lithium alkoxide (ROLi) and Li_2CO_3 products.[6, 7]

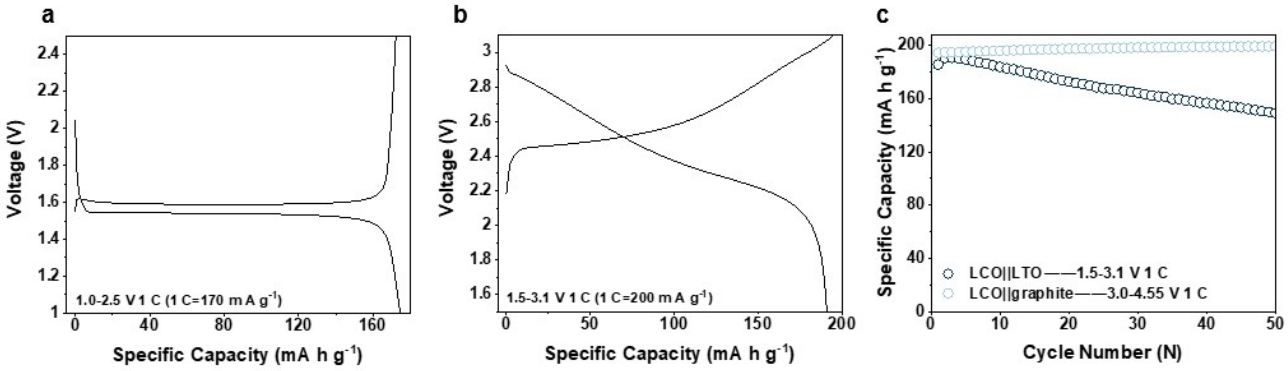

Fig. S31 Charge and discharge curves of a) LTO||Li half cells within a voltage range of 1.0-2.5 V at 1 C, and b) LCO||LTO full cells within a voltage range of 1.5-3.1 V at 1 C in FEC-DFEC electrolyte. c) Cycling performance of LCO||LTO coin cells within a voltage range of 1.5-3.1 V at 1 C, and LCO||graphite coin cells within a voltage range of 3.0-4.55 V at 1 C.

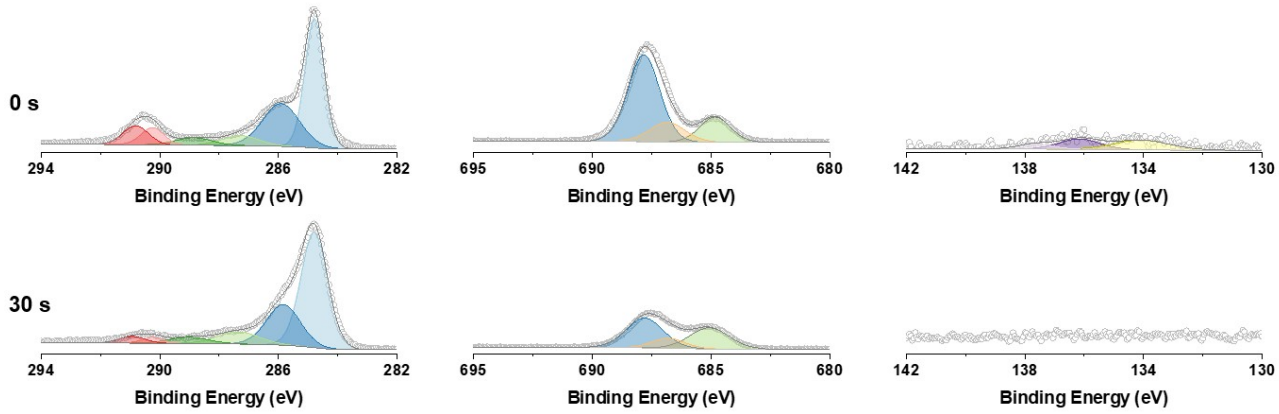

Fig.S32 The C 1s, F 1s, and P 2p XPS spectra of the LCO cathode electrode with different etching time after 50 cycles of LCO||LTO cells within a voltage range of 1.5-3.1 V at 1 C in FEC-DFEC electrolytes.

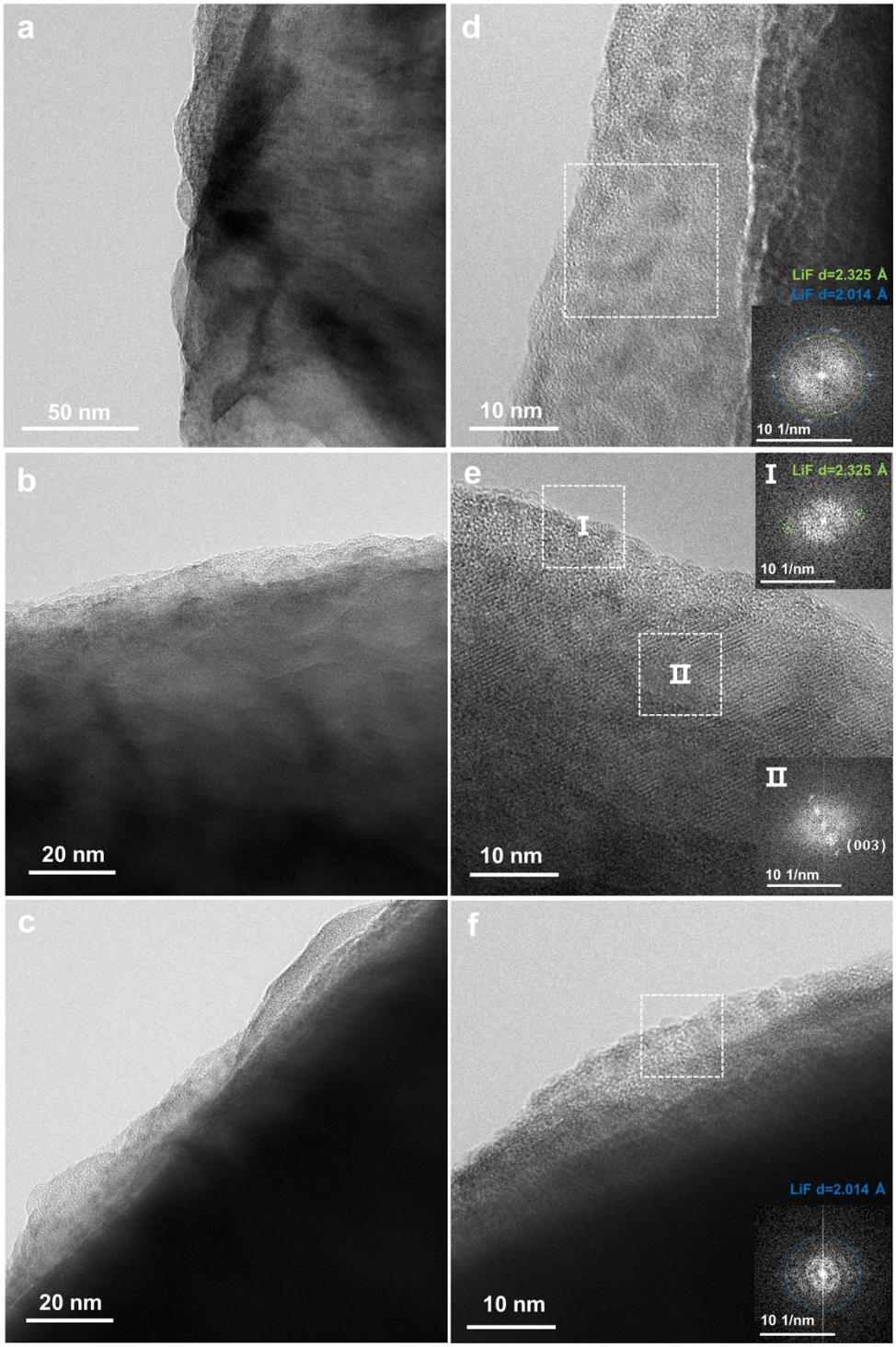

Fig.S33 a,b,c) The cryo-TEM images of LCO after 50 cycles of LCO||LTO cells within a voltage range of 1.5-3.1 V at 1 C in FEC-DFEC electrolyte, d,e,f) and corresponding enlarged images and FFT.

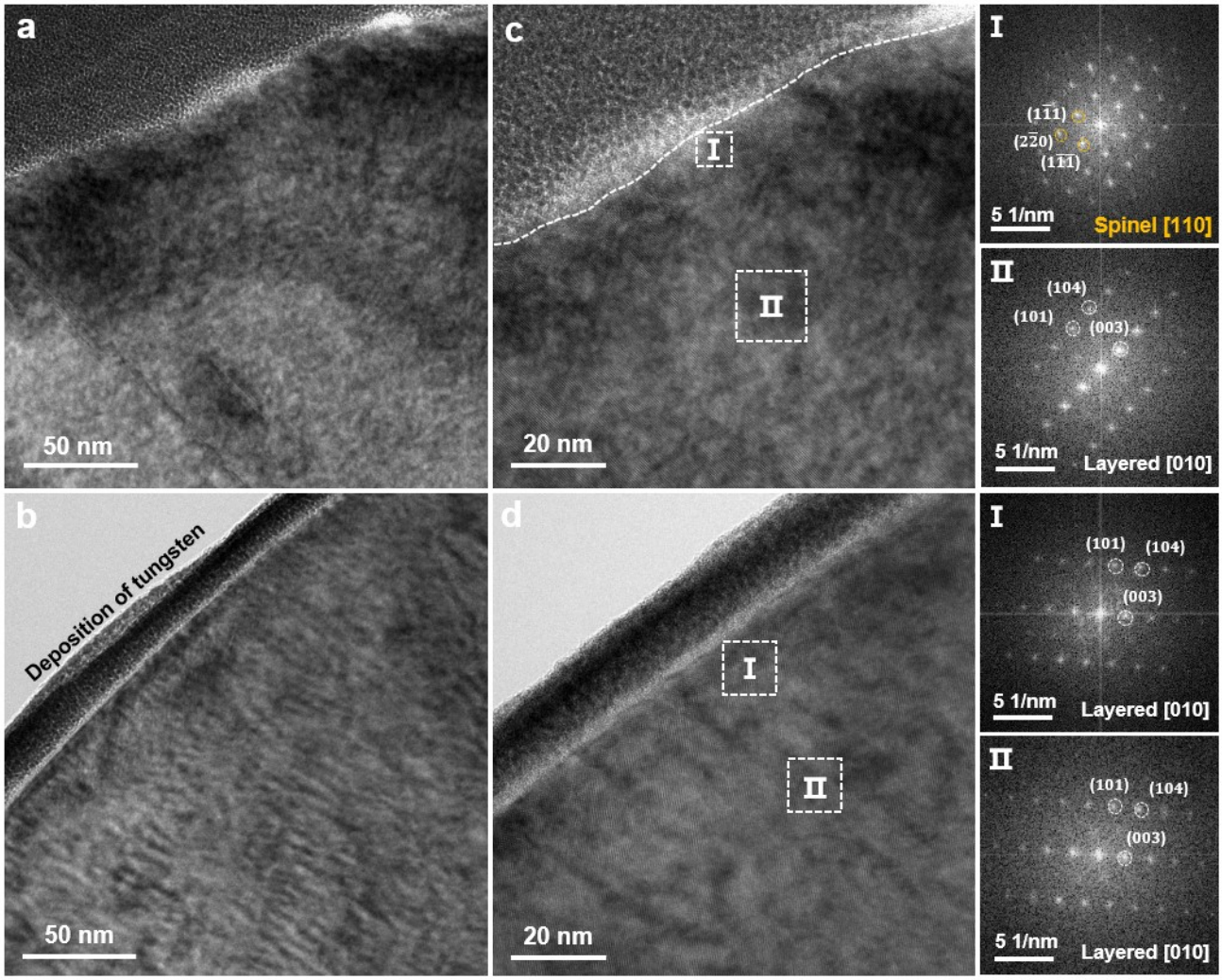

Fig. S34 The high-resolution TEM images of LCO at 4.6 V charged state in the first cycle in a) EC electrolyte and b) FEC-DFEC electrolyte, with the charge current of 0.2 C, and c,d) the corresponding enlarged images with FFT results.

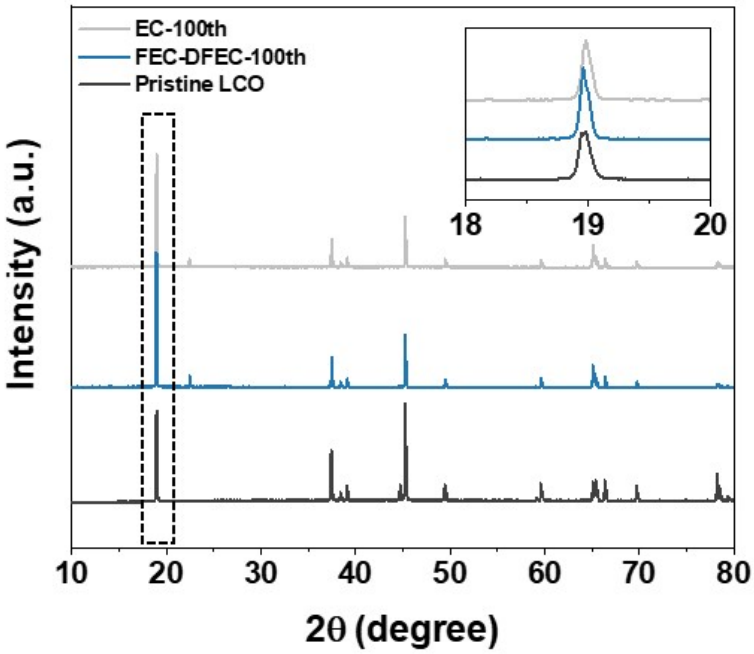

Fig. S35 The comparison of XRD diffraction for pristine LCO electrode, LCO electrode in EC electrolyte and LCO electrode in FEC-DFEC electrolyte of LCO||Li cells after 100 cycles.

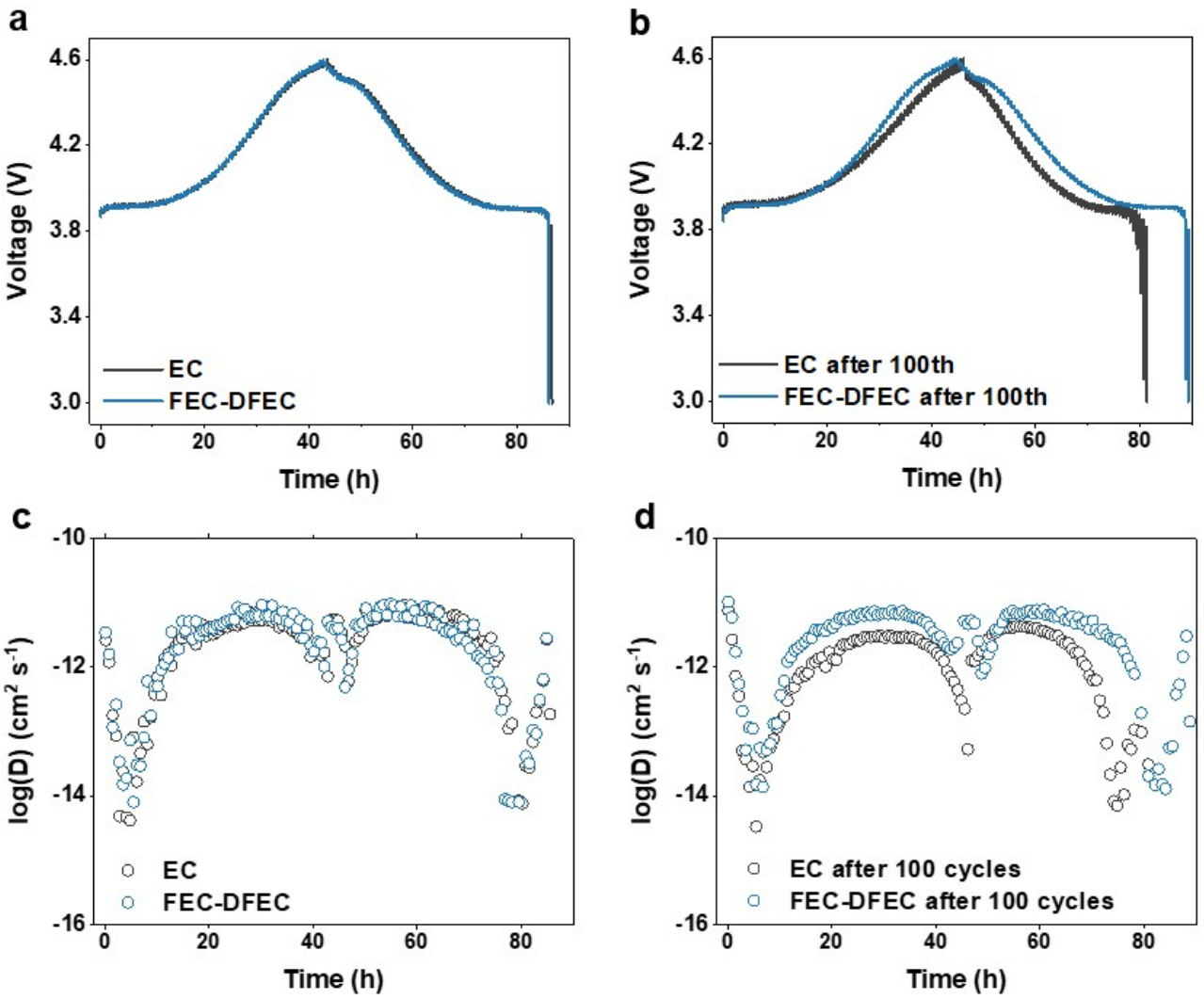

Fig. S36 The GITT measurements curves of LCO||Li half cells within a voltage range of 3.0-4.6 V in EC and FEC-DFEC electrolytes. a) after 2 cycles at 0.2 C and b) after 100 cycles at 1 C. The calculated Li^+ diffusion coefficient of LCO in EC and FEC-DFEC electrolytes c) after 2 cycles at 0.2 C and d) after 100 cycles at 1 C.

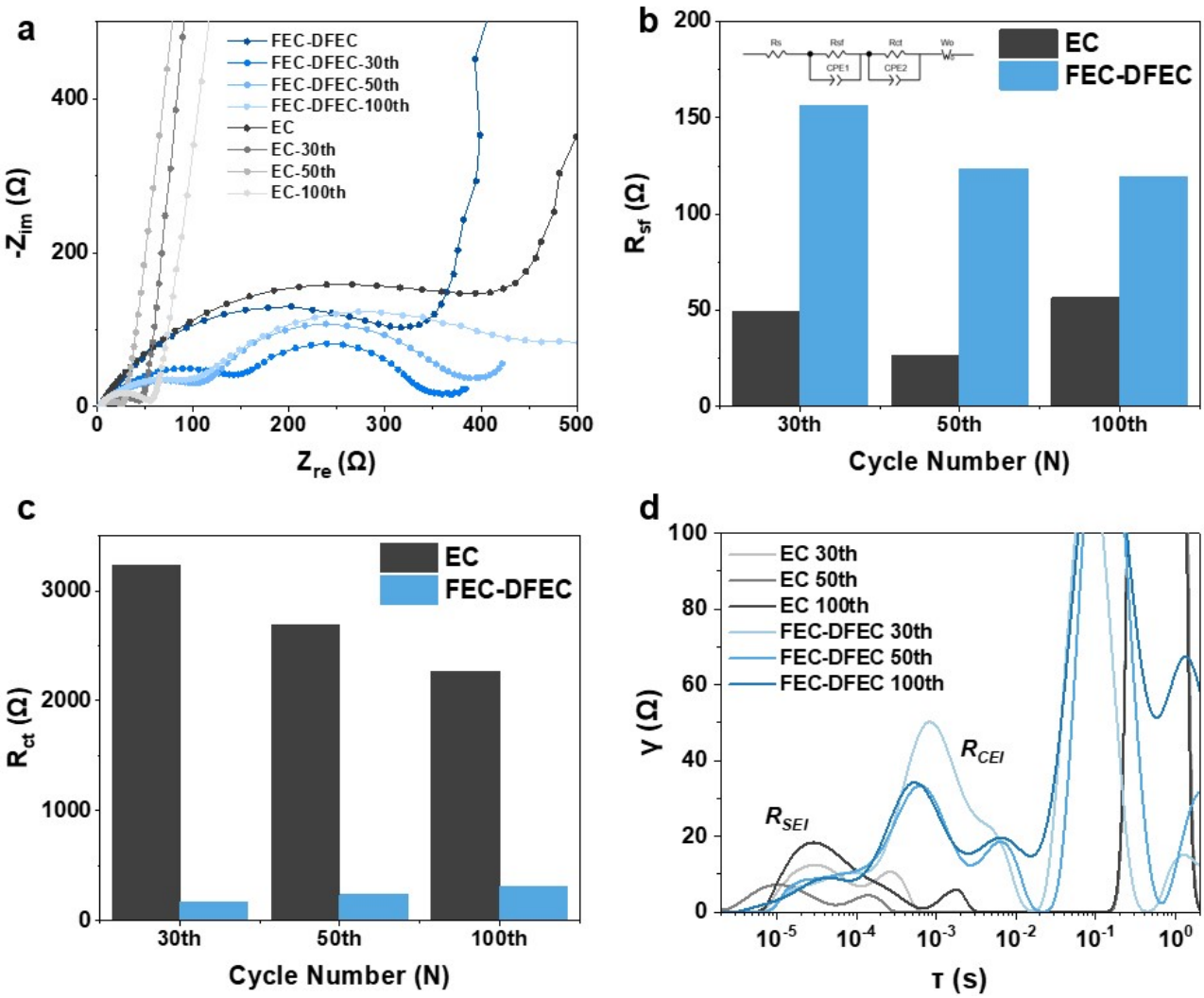

Fig. S37 a) The EIS measurements of LCO||Li half cells within a voltage range of 3.0-4.6 V in EC and FEC-DFEC electrolytes. The corresponding fitting results of b) R_{sf} and c) R_{ct} by equivalent circuit. d) The distribution of relaxation time (DRT) curve extracted by Fourier transform of above EIS results after different cycles.

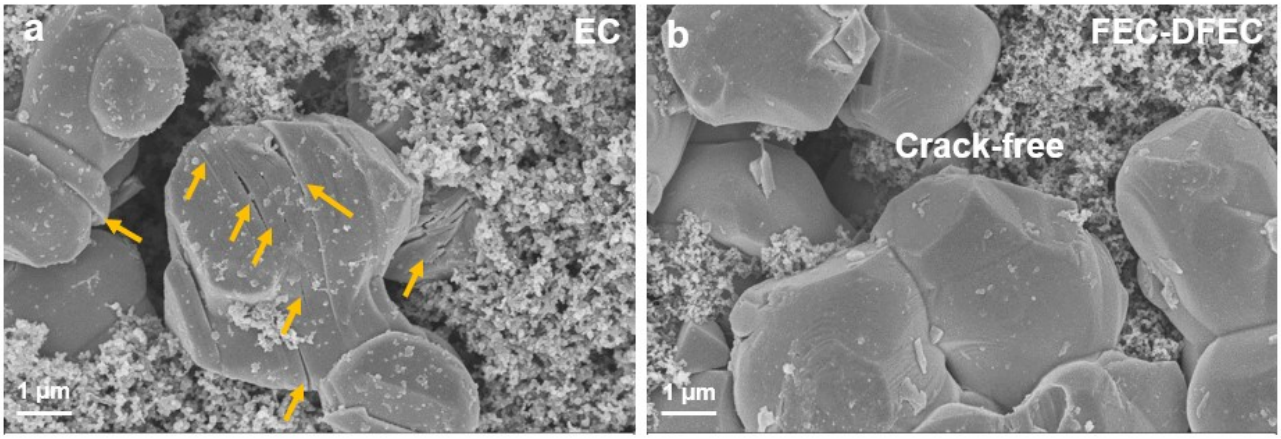

Fig. S38 SEM images of LCO cathode electrode after 100 cycles of LCO||Li half cells within a voltage range of 3.0-4.6 V at 1 C in a) EC and b) FEC-DFEC electrolytes.

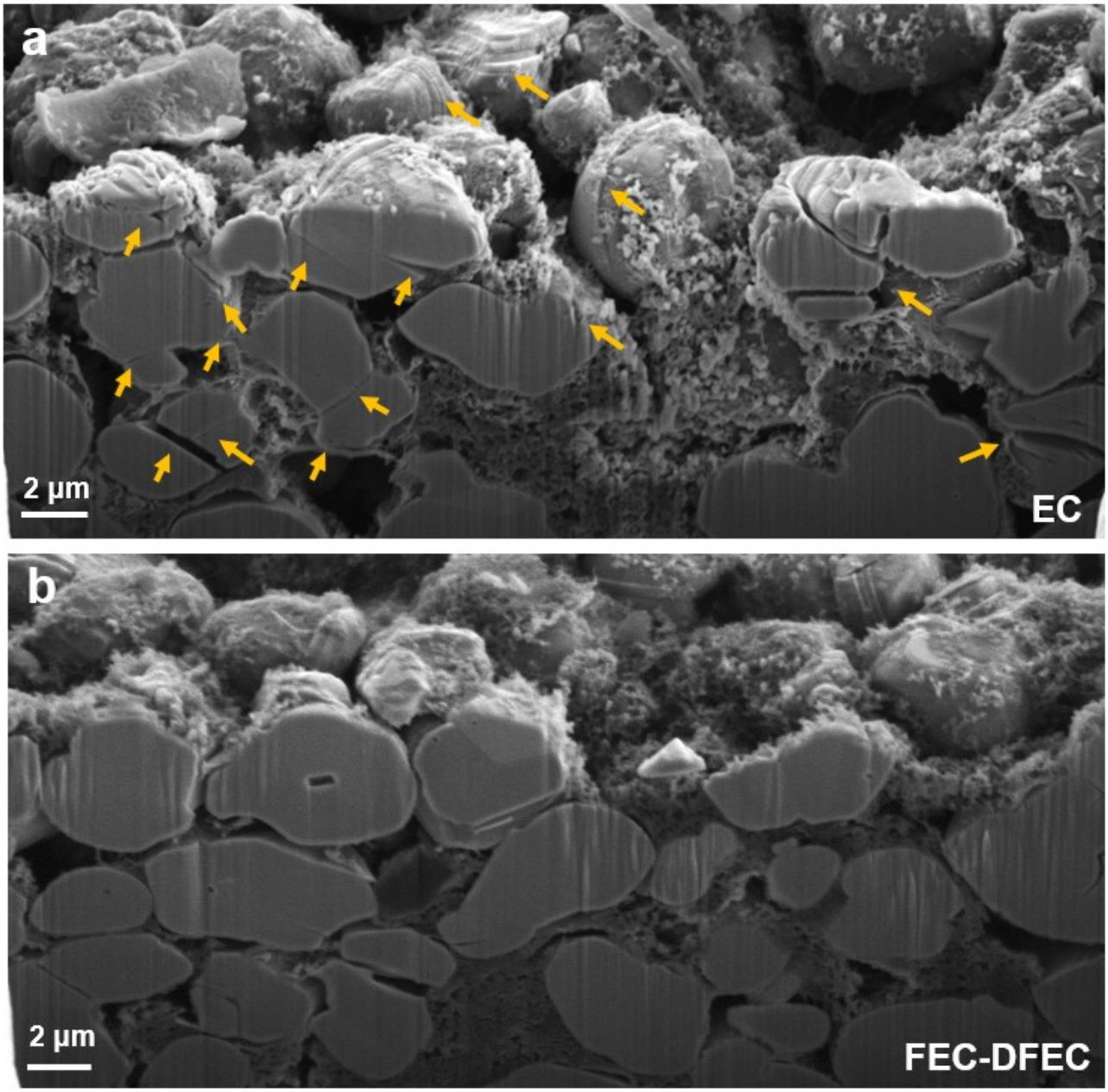

Fig. S39 Cross-section SEM images of LCO cathode electrode after 500 cycles of LCO||graphite pouch full cells within a voltage range of 3.0-4.55 V at 1 C in a) EC and b) FEC-DFEC electrolytes.

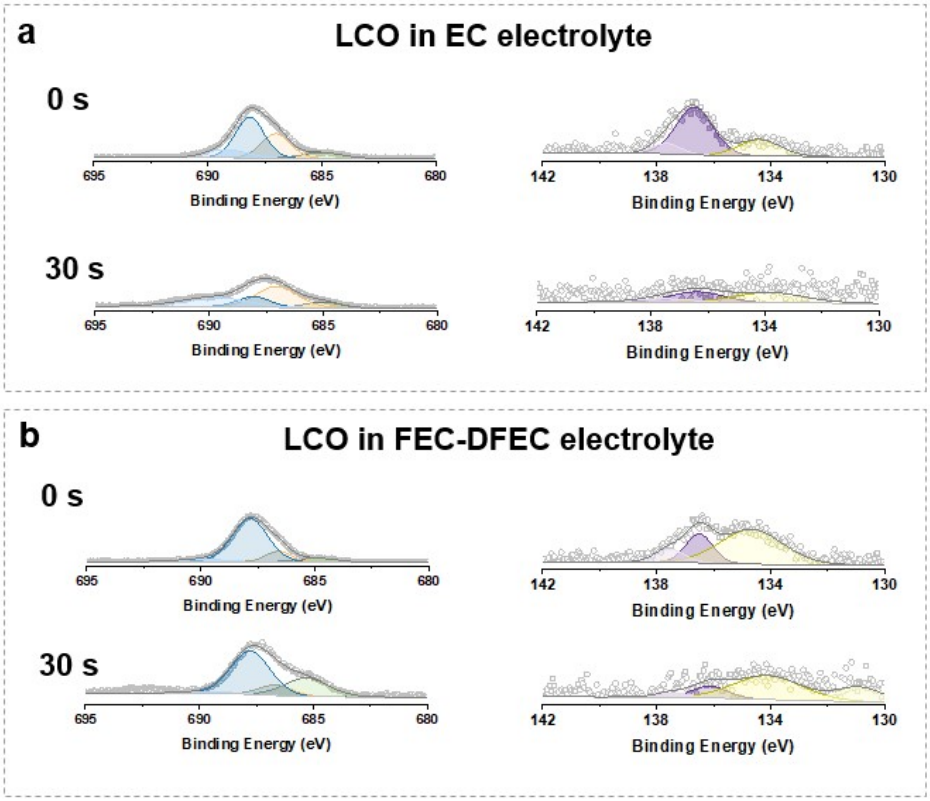

Fig. S40 The F 1s and P 2p XPS spectra of the LCO surface with different etching time after 500 cycles of LCO||graphite pouch full cells within a voltage range of 3.0-4.55 V at 1 C in a) EC and b) FEC-DFEC electrolytes.

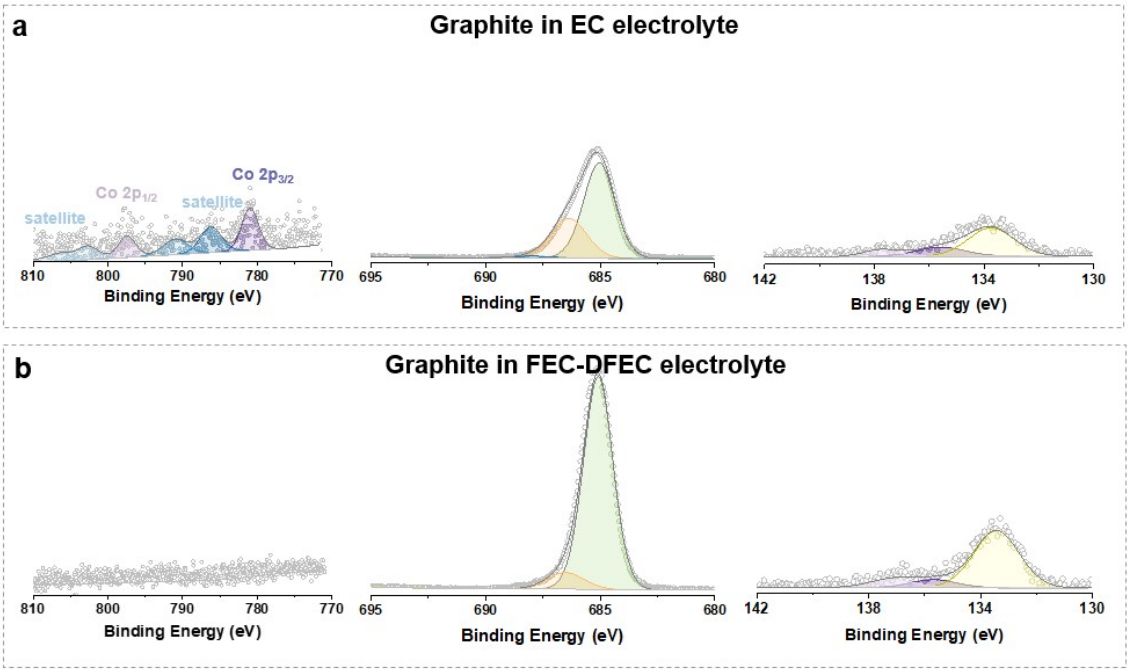

Fig. S41 The Co 2p, F 1s and P 2p XPS spectra of the graphite surface after 500 cycles of LCO||graphite pouch full cells within a voltage range of 3.0-4.55 V at 1 C in a) EC and b) FEC-DFEC electrolytes.

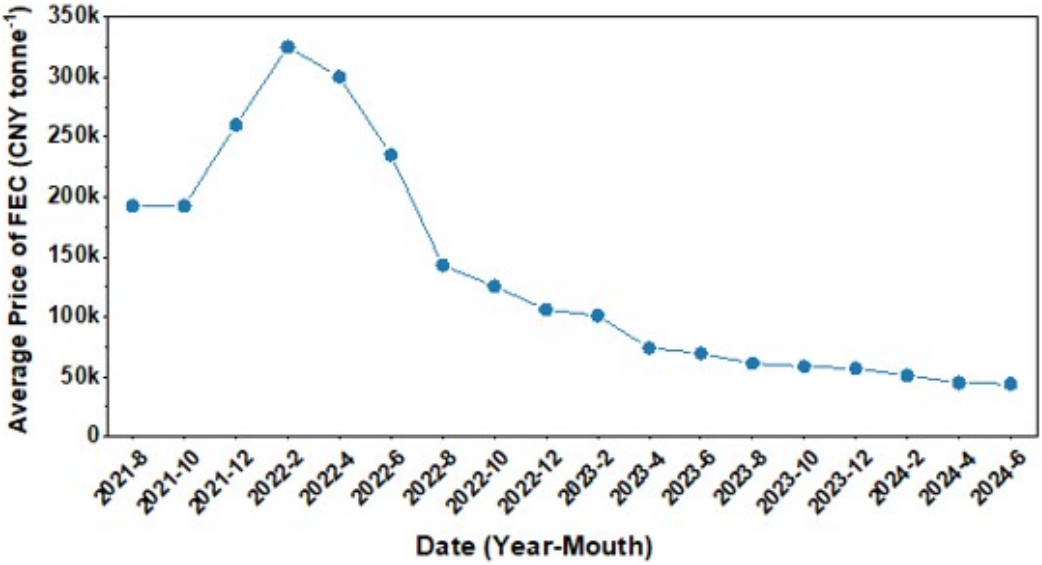

Fig. S42 The price trend of FEC in recent 4 years.

Table S1 Five kinds of electrolytes solvents composition (by volume ratio).

Electrolyte	Composition
EC	1.0 M $LiPF_6$ in EC/EMC (3:7)
EC-DEC	1.0 M $LiPF_6$ in EC/EMC/DEC (3:4:3)
FEC	1.0 M $LiPF_6$ in FEC/EMC/DEC (3:4:3)
FEC-DFEC	1.0 M $LiPF_6$ in DFEC/FEC/EMC/DEC (1.5:1.5:4:3)
DFEC	1.0 M $LiPF_6$ in DFEC/EMC/DEC (3:4:3)

Table S2 Electrochemical performance comparison of recently reported electrolyte regulation for LCO cathode at room temperature.

Electrolyte composition	Electrochemical performance	Ref.
1.0 M $LiPF_6$ in FEC/FEMC/TTE + TMSB additive	LCO||Li coin cell: 3.0-4.6 V 0.5 C 300th 74.8%; 0.2 C 222 mA h g^{-1}, 10 C 98 mA h g^{-1}; LCO||graphite coin cell: 3.0-4.5 V 0.5 C 500th 80%; LCO||graphite pouch cell (120 mA h): 3.0-4.5 V 0.3 C 200th 77.5%.	[8]
1.3 M LiFSI in DME/TFEE + 1% LiFMDFB + 0.05% $AgNO_3$	LCO||Li coin cell: 3.0-4.4 V 0.5 C 200th 84.5%; 3.0-4.5 V 0.5 C 100th 94.5%	[9]
1.0 M $LiPF_6$ in EC/EMC/DMC + 1.5 wt% TPFPB + 5 wt% LiDFBP mixture	LCO||Li coin cell: 2.7-4.6 V 1 C 400th 80.1%, 1000th 51.0%; 0.2 C 207 mA h g^{-1}, 5 C ≈140 mA h g^{-1}	[10]
1.0 M $LiPF_6$ in FEMC/DFEC/FEC/TTE + 0.02 M $LiPO_2F_2$,	LCO||Li coin cell: 3.0-4.6 V 1 C 500th 84.1%, 3 C 1000th 77.6%, 5 C 1000th 73.2%; 5 C 160 mA h g^{-1}, 10 C 140 mA h g^{-1} LCO||graphite coin cell: 3.0-4.55 V 3 C 1000th 64.5%; LCO||graphite pouch cell (184 mA h): 3.0-4.55 V 290 mA 500th 85.5%.	[11]
1.0 M $LiPF_6$ in FEC/DFEC/DMC	LCO||Li coin cell: 3.0-4.6 V 0.3 C 100th 91%, 3.0-4.6 V 0.5 C 500th 78%,0.3 C 220 mA h g^{-1}, 5 C 140 mA h g^{-1}	[12]
1 M LiFSI in $DMCF_3SA$	LCO||Li coin cell: 3.0-4.55 V charge at 50 mA h g^{-1} and discharge at 150 mA h g^{-1} 200th 89%, 3.0-4.6 V 100th 85%	[13]
1.0 M $LiPF_6$ in DEC/EC/EMC +1% DPD-F	LCO||Li coin cell: 3.0-4.5 V 0.3 C 400th 87.9%, 3.0-4.6V 200th 69.2%	[14]
1.0 M $LiPF_6$ in EC/DEC + 0.5wt% SPTF additive	LCO||Li coin cell: 3.0-4.65 V 1 C 300th 70.3%, charge at 1 C and discharge at 2 C 1000th 88.2%, LCO||graphite coin cell: 0.5 C 200th 83.6%; LCO||graphite pouch cell (1.03 A h):.0.5 C 200th 99.3%. LCO/SiO pouch cell (1.455 A h): .0.5 C 400th 80.4%.	[15]
1.3 M $LiPF_6$ in EC/PC/EB + 7% FEC + 1% LiFMDFB + 3% HTCN + 0.2% TMSP	LCO||graphite coin cell: 3.0-4.55 V charge at 1.5 C and discharge at 0.5 C 500th 51.8%.	[16]
1.0 M $LiPF_6$ in DFEC/FEC/EMC/DEC	**LCO||Li coin cell: 3.0-4.6 V 1 C 500th 92.7%; 2 C 1000th 85.5%, 0.2 C 220 mA h g^{-1}, 8 C 173.9 mA h g^{-1}; LCO||graphite pouch cell (0.6 A h): 3.0-4.55 V 1 C 500th 85.7%.**	**This work**

Table S3 A brief summary of the synthesis technology of FEC/DFEC.

Synthesis technology		Synthesis process schematic	Features and Environment impact
Halogen exchange reaction method (widely used)	The chloroethylene carbonate turn into FEC/DFEC by a fluorinating reagent (NaF, KF, HF, etc.) under a nucleophilic substitution reaction in the organic solvent. The key factors affecting the productive rate are the selection of phase transfer catalyst (ionic liquid, quaternary ammonium saltand, crown ether, etc.) and advanced purification technology (removal of water, acid and halogen ions etc., followed by distillation process). [17, 18]	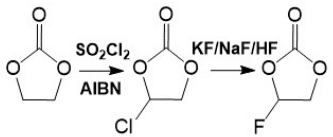	1). Relatively complicated preparation and purification process; 2). Overall consideration of the cost, reaction selectivity and stability of the catalyst; 3). Low demand in equipment and high safety during operation; 4). High production of industrial waste liquid, gas, solid, which require corresponding treatment methods.
Direct fluorination method	FEC/DFEC can be produced by the substitution reaction of EC with F_2 gas. Two methods can be used to avoid the heat accumulation during the fluorination reaction: 1) use another solvent to dilute EC, 2) use diluted fluorine gas (F_2/N_2). The production rate is highly related to the reactor selection (tank reactor or microchannel reactor), temperature, pressure, F_2 concentration, etc.[19]	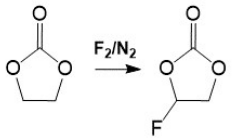	1). Due to the highly reactive, corrosive, toxic F_2 gas, and heat release during fluorination, the production process propose a higher demand for the equipments and operation; 2). Low production rate with plenty of fluorinated by-products; 3). Harmful effects of F_2 and HF to environment, which require corresponding treatment methods.
Electrochemical fluorination method	Electrochemical fluorination (anodic fluorination) is one of the most promising industrial fluorination technology. The reaction process of VC to FEC is shown in the schematic. The electrolytic solvents, fluorinated agents, and work electrodes significantly affect the selectivity and efficiency of fluorination.[20, 21]	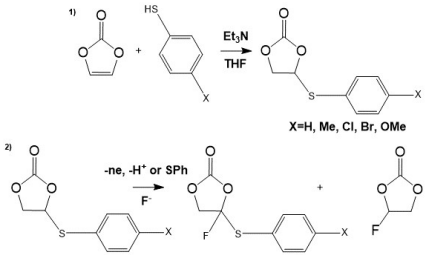	1). High technical difficulty; 2). The fluorinated process is more economical with high production rates; 3). Low demand in equipment and easy to operation.

Table S4 A brief summary of the recycling technology of electrolytes.

Electrolyte recycling technology		Recycling process	Features
Low temperature thermal treatment methode	According to the boiling point and flash point of each component in the electrolyte, recover the electrolyte by distillation and condensation process.	The low treatment process of disassembled battery is under 130 ℃ for 80 min. The organic solvents included linear and cyclic carbonates DMC, EMC and EC etc. in the electrolyte are successfully recovered in liquid phase. Using gas washing bottles filled with water to recycle the corrosive HF and POF_3 gas.[22]	1). Low-cost and controllable; 2). The recycling of involatile lithium salt is relatively difficult.
		Use a low temperature vacuum evaporation drying-condensation method to separate and recover the electrolyte. The electrodes are dried in vacuum 140 ℃ for 4 h, and the steam is recovered after being condensed at 0/-20/-50/-75 ℃ in turn. The condensate containe pure EC, DMC, EMC and DEC etc organic solvents.[23]	
		By applying the 120 ℃ volatilization, approximately 99.91% of organic electrolytes can be recycled, and the $LiPF_6$ is disposed by pyrolytic process, under N_2 atmosphere at 550 ℃ for 2 h.[24]	
Solvent extraction method	Use the organic solvent to extract the electrolyte from battery, and vacuum distillation to recover organic solvent and lithium salt.	The disassembled battery electrodes are placed in an organic solvent to extract the electrolyte, then the liquid is went through vacuum concentration, cooling and crystallization to recover the organic solvents and lithium salt.	1). The introduction of new organic reagents and loss of extractant can cause waste organics pollution and increase the cost of recovery; 2). High recovery efficiency.
Supercritical CO_2 extraction method	Supercritical CO_2 can dissolve non-polar substance, and effectively extract electrolyte from waste lithium-ion batteries. Operation processes are relatively mild and suitable for extracting heat sensitive substances, such as $LiPF_6$.	Extraction with transcritical CO_2 is a suitable method with moderate conditions to recover the organic carbonate solvents of LIB electrolytes. Extraction pressure is the major factor contributing to electrolyte extraction and the extraction yield is 85.07+0.36% under the operating conditions of 23 MPa, 40 °C, and 45 min.[25]	1). High requirements to the equipment; 2). High-cost and limiting of industrialization; 3) High recovery efficiency and environment-friendly.
		Extraction conditions is under 40 °C and 15 MPa, the experiment begin with a static extraction step which is held for 10 min, followed by 20 min of dynamic extraction with a constant flow rate of 2.0 $L \cdot min^{-1}$. An extraction yield of about 85% can be achieved.[26]	

Chemical conversion method	By introducing reagents such as NaOH, KOH, H_2SO_4 etc., the chemical conversion of electrolyte can produce more stable lithium salts (e.g. $LiPO_2F_2$, Li_2CO_3, etc.), followed by the distillation, filtration etc. process.	A special complex aqueous peeling agent, namely exfoliating and extracting solution (AEES) is manufactured and applied in this process. EC and PC etc. organic can be extracted from electrodes and separators and recovered via distillation. $LiPF_6$ can reacted with AEES to form water soluble lithium salt and $NaPF_6$, then be precipitated from solution and recovered via filtration.[27]	1). High recovery efficiency of lithium salt but low recovery efficiency of organic solvents; 2). The introduction of new reagents can cause waste pollution and increase the cost of recovery;
		Lithium carbonate preparation from a lithium-rich electrolyte by H_2SO_4 leaching, followed by purification and precipitation. About 98% Li leaching efficiency is achieved in 1 h using 6% H_2SO_4 at 80 °C. Li_2SO_4 in the resulting leach solution is sequentially purified by NaOH addition to an end pH of 11 and then addition of 3 g/L ethylenediaminetetraacetic acid. Li_2CO_3 of 99.5% purity is then obtained by precipitation with addition of 290 g/L Na_2CO_3 at 95 °C for 50 min.[28]	

References

1. A. D. Becke, *J. Chem. Phys.*, 1993, **98**, 5648-5652.
2. C. Lee, W. Yang and R. G. Parr, *Phys. Rev. B*, 1988, **37**, 785-789.
3. R. Krishnan, J. S. Binkley, R. Seeger and J. A. Pople, *J. Chem. Phys.*, 1980, **72**, 650-654.
4. A. V. Marenich, C. J. Cramer and D. G. Truhlar, *J. Phys. Chem. B*, 2009, **113**, 6378-6396.
5. Y.-C. Lu, A. N. Mansour, N. Yabuuchi and Y. Shao-Horn, *Chem. Mater.*, 2009, **21**, 4408-4424.
6. Y. Zhang, D. Krishnamurthy and V. Viswanathan, *J. Electrochem. Soc.*, 2020, **167**, 070554.
7. D. Aurbach, E. Markevich and G. Salitra, *JACS*, 2021, **143**, 21161-21176.
8. J. Zhang, P. F. Wang, P. Bai, H. Wan, S. Liu, S. Hou, X. Pu, J. Xia, W. Zhang, Z. Wang, B. Nan, X. Zhang, J. Xu and C. Wang, *Adv. Mater.*, 2022, **34**, 2108353.
9. S. Kim, J.-A. Lee, T. K. Lee, K. Baek, J. Kim, B. Kim, J. H. Byun, H.-W. Lee, S. J. Kang, J.-A. Choi, S.-Y. Lee, M.-H. Choi, J.-H. Lee and N.-S. Choi, *Energy Environ. Sci.*, 2023, **16**, 5108-5122.
10. H. Zhang, Y. Huang, Y. Wang, L. Wang, Z. Song, H. Wang, C. Xu, X. Tian, S. Wang, J. Fang, W. Zhao, H. Cao, X. Yao, J. Yang, R. Tan, L. Yang, F. Pan and Y. Zhao, *Energy Storage Mater.*, 2023, **62**, 102951.
11. A. Zhang, Z. Bi, G. Wang, S. Liao, P. Das, H. Lin, M. Li, Y. Yu, X. Feng, X. Bao and Z.-S. Wu, *Energy Environ. Sci.*, 2024.
12. T. Fan, W. Kai, V. K. Harika, C. Liu, A. Nimkar, N. Leifer, S. Maiti, J. Grinblat, M. N. Tsubery, X. Liu, M. Wang, L. Xu, Y. Lu, Y. Min, N. Shpigel and D. Aurbach, *Adv. Funct. Mater.*, 2022, **32**, 2204972.
13. W. Xue, R. Gao, Z. Shi, X. Xiao, W. Zhang, Y. Zhang, Y. G. Zhu, I. Waluyo, Y. Li, M. R. Hill, Z. Zhu, S. Li, O. Kuznetsov, Y. Zhang, W.-K. Lee, A. Hunt, A. Harutyunyan, Y. Shao-Horn, J. A. Johnson and J. Li, *Energy Environ. Sci.*, 2021, **14**, 6030-6040.
14. Z. Sun, F. Li, J. Ding, Z. Lin, M. Xu, M. Zhu and J. Liu, *ACS Energy Lett.*, 2023, **8**, 2478-2487.
15. Y. Yan, S. Weng, A. Fu, H. Zhang, J. Chen, Q. Zheng, B. Zhang, S. Zhou, H. Yan, C.-W. Wang, Y. Tang, H. Luo, B.-W. Mao, J. Zheng, X. Wang, Y. Qiao, Y. Yang and S.-G. Sun, *ACS Energy Lett.*, 2022, **7**, 2677-2684.
16. S. Kim, J.-A. Lee, D. G. Lee, J. Son, T. H. Bae, T. K. Lee and N.-S. Choi, *ACS Energy Lett.*, 2023, **9**, 262-270.
17. C. Zheng, J. Wu, L. Zhang and H. Wang, *J. Mater. Chem. C*, 2023, **11**, 344-363.
18. G. Ma, L. Wang, J. Zhang, H. Chen, X. He and Y. Ding, *Prog. Chem.*, 2016, **28**, 1299-1312.
19. M. Hill, P. Baron, K. Cobry, S. K. Goll, P. Lang, C. Knapp, H. Scherer, P. Woias, P. Zhang and I. Krossing, *ChemPlusChem*, 2013, **78**, 292-301.
20. H. Ishii, N. Yamada and T. Fuchigami, *TETRAHEDRON*, 2001, **57**, 9067-9072.
21. Y. Wang, Z. Li, Y. Hou, Z. Hao, Q. Zhang, Y. Ni, Y. Lu, Z. Yan, K. Zhang, Q. Zhao, F. Li and J. Chen, *Chem. Soc. Rev.*, 2023, **52**, 2713-2763.
22. N. Zachmann, M. Petranikova and B. Ebin, *J. Ind. Eng. Chem.*, 2023, **118**, 351-361.
23. C. Song, R. Dingshan, Z. You and L. Qiang, *Battery Bimonthly*, 2022, **52**, 114-117.
24. X. Zhong, W. Liu, J. Han, F. Jiao, W. Qin, T. Liu and C. Zhao, *Waste Manage. (Oxford)*, 2019, **89**, 83-93.
25. D. Mu, Y. Liu, R. Li, Q. Ma and C. Dai, *New J. Chem.*, 2017, **41**, 7177-7185.
26. Y. Liu, D. Mu, R. Li, Q. Ma, R. Zheng and C. Dai, *J. Phys. Chem. C*, 2017, **121**, 4181-4187.
27. K. He, Z.-Y. Zhang, L. Alai and F.-S. Zhang, *J. Hazard. Mater.*, 2019, **375**, 43-51.
28. W. Wang, W. Chen and H. College, *Hydrometallurgy*, 2019, **185**, 88-92.